cmgh
CELLULAR AND MOLECULAR GASTROENTEROLOGY AND HEPATOLOGY

ORIGINAL RESEARCH

Gut Bacteria-derived Membrane Vesicles Induce Colonic Dysplasia by Inducing DNA Damage in Colon Epithelial Cells

Yu Miyakawa,[1] Motoyuki Otsuka,[1,2] Chikako Shibata,[1] Takahiro Seimiya,[1] Keisuke Yamamoto,[1] Rei Ishibashi,[1] Takahiro Kishikawa,[1] Eri Tanaka,[1] Takayuki Isagawa,[3] Norihiko Takeda,[3,4] Noriaki Kamio,[5] Kenichi Imai,[5] and Mitsuhiro Fujishiro[1]

[1]*Department of Gastroenterology, Graduate School of Medicine, The University of Tokyo, Tokyo, Japan;* [2]*Department of Gastroenterology and Hepatology, Academic Field of Medicine, Density and Pharmaceutical Sciences, Okayama University, Okayama, Japan;* [3]*Division of Cardiology and Metabolism, Center for Molecular Medicine, Jichi Medical University, Tochigi, Japan;* [4]*Department of Cardiovascular Medicine, Graduate School of Medicine, The University of Tokyo, Tokyo, Japan; and* [5]*Department of Microbiology and Immunology, Nihon University School of Dentistry, Tokyo, Japan*

SUMMARY

This study investigates *Actinomyces odontolyticus*'s role in colorectal cancer initiation. The bacterium secretes lipoteichoic acid-rich membrane vesicles, inducing chronic inflammation, nuclear factor kappa B signaling, and excessive reactive oxygen species in colonic epithelial cells. These processes result in DNA damage, potentially contributing to colorectal cancer development.

BACKGROUND & AIMS: Colorectal cancer (CRC) is the third most common cancer in the world. Gut microbiota has recently been implicated in the development of CRC. *Actinomyces odontolyticus* is one of the most abundant bacteria in the gut of patients with very early stages of CRC. *A odontolyticus* is an anaerobic bacterium existing principally in the oral cavity, similar to *Fusobacterium nucleatum,* which is known as a colon carcinogenic bacterium. Here we newly determined the biological functions of *A odontolyticus* on colonic oncogenesis.

METHODS: We examined the induction of intracellular signaling by *A odontolyticus* in human colonic epithelial cells (CECs). DNA damage levels in CECs were confirmed using the human induced pluripotent stem cell-derived gut organoid model and mouse colon tissues in vivo.

RESULTS: *A odontolyticus* secretes membrane vesicles (MVs), which induce nuclear factor kappa B signaling and also produce excessive reactive oxygen species (ROS) in colon epithelial cells. We found that *A odontolyticus* secretes lipoteichoic acid-rich MVs, promoting inflammatory signaling via TLR2. Simultaneously, those MVs are internalized into the colon epithelial cells, co-localize with the mitochondria, and cause mitochondrial dysfunction, resulting in excessive ROS production and DNA damage. Induction of excessive DNA damage in colonic cells by *A odontolyticus*-derived MVs was confirmed in the gut organoid model and also in mouse colon tissues.

CONCLUSIONS: *A odontolyticus* secretes MVs, which cause chronic inflammation and ROS production in colonic epithelial cells, leading to the initiation of CRC. *(Cell Mol Gastroenterol Hepatol 2024;17:745–767; https://doi.org/10.1016/j.jcmgh.2024.01.010)*

Keywords: A odontolyticus; DNA Damage; NF-κB; Colon Cancer; Mitochondria.

Colorectal cancer (CRC) is the third most common cancer in the world, with approximately 1.9 million new cases per year.[1] Although CRC is a multifactorial disease, most of them occur sporadically in combination with genetics and environmental factors such as chronic inflammation or diet habits.[2] Most cases are preceded by dysplastic adenomas, which can progress into malignant forms through the accumulation of genetic mutations.[3]

Recently, growing evidence shows that gut microbiota has been implicated in the development of CRC.[4] Approximately 3×10^{13} bacteria are present in the human colorectum, interacting with many microorganisms and intestinal epithelial cells in constant crosstalk.[5] Such microbiota has been suggested to play crucial roles in the development of CRC by inducing chronic inflammation and DNA damages.[6] Since the first report about the association between *Fusobacterium nucleatum* and CRC in 2012,[7,8] numerous studies have been done to clarify their association and oncogenic mechanisms.[9] Besides *F nucleatum*, other bacterial species such as enterotoxigenic *Bacteroides fragilis*, pathogenic *Escherichia coli*, and *Peptostreptococcus* spp. have also been reported to be associated with the development of CRC.[10]

A recent comprehensive study identified *Actinomyces odontolyticus* as one of the abundant bacteria in the stools of

Abbreviations used in this paper: **ANOVA, analysis of variance; A.o MV, *Actinomyces odontolyticus* membrane vesicle; CRC, colorectal cancer; DMEM, Dulbecco modified Eagle medium; DNM, dynamin; EHEC, enterohemorrhagic *E coli*; EV, extracellular vesicle; iCEC, SV40-immortalized human colon epithelial cell; IL, interleukin; iPSC, induced pluripotent stem cell; LTA, lipoteichoic acid; mtDNA, mitochondrial DNA; MV, membrane vesicle; NF-κB, nuclear factor kappa B; OCR, oxygen consumption rate; OMV, outer membrane vesicle; OXPHOS, oxidative phosphorylation; PBS, phosphate-buffered saline; ROS, reactive oxygen species; SD, standard deviation; SDS, sodium dodecyl sulfate; TLR, toll-like receptor; TNF, tumor necrosis factor.**

Most current article

2352-345X
https://doi.org/10.1016/j.jcmgh.2024.01.010

patients with very early stages of CRC.[11] *A odontolyticus*, which was isolated from dental caries in 1958, is a facultative anaerobic bacterium existing mainly in oral cavity, genital, and gastrointestinal tracts[12] and is closely associated with periodontitis, similar to *F nucleatum*.[13] However, its biological functions on the early CRC or the colonic oncogenesis are unclear.

In this study, we hypothesized that *A odontolyticus* is involved in the initiation of CRC. Whereas it has been recently proposed that gut microbiota produces extracellular vesicles (EVs), called membrane vesicles (MVs), we here show that MVs released from *A odontolyticus* are involved in the initiation of CRC.

Results

A odontolyticus Activates the Nuclear Factor Kappa B Signaling Pathway in Human Colon Epithelial Cells

Because nuclear factor kappa B (NF-κB) signaling pathway is a representative driver of tumorigenesis by *F nucleatum,*[14] we hypothesized that *A odontolyticus* may also activate this pathway. To examine this hypothesis, we performed a co-culture using immortalized human colon epithelial cells (iCECs) with *A odontolyticus*, *F nucleatum*, *E coli* DH5α, or phosphate-buffered saline (PBS) (Figure 1*A*). Similar to the cases of *F nucleatum*, IκBα was significantly degraded and phosphorylation levels of IκBα were significantly increased by *A odontolyticus,* compared with those by *E coli* DH5α or PBS control (Figure 1*B*). Higher levels of NF-κB subunit p65 were translocated into the nuclei by both *A odontolyticus* and *F nucleatum* than those by *E coli* DH5α or PBS control (Figure 1*C*). Furthermore, mRNA levels of interleukin (IL) 8 and tumor necrosis factor (TNF) α, upregulated by NF-κB activation, were also significantly increased by *A odontolyticus* and *F nucleatum,* compared with those by *E coli* DH5α or PBS control (Figure 1*D*).

A odontolyticus Secretes Membrane Vesicles, Promoting Inflammatory Signaling in Colon Epithelial Cells

In the case of *F nucleatum*, its multiple adhesin molecules such as FadA or Fap2 cause pathogenesis involving modification of innate immunity or tumor progression due to the attachment to the host cells such as colorectal cancer cells or T cells.[15–17] On the basis of these, we first examined whether *A odontolyticus* attaches to iCECs or colorectal cancer cell lines HCT116 and HT29, using previously reported attachment assays.[17,18] In human iCECs, the attachment rates of *A odontolyticus* were significantly lower than those of *F nucleatum* and were not significantly different from those of *E coli* DH5α (Figure 2*A*). Similar results were revealed in HCT116 and HT29 (Figure 2*A*).

To further investigate whether *A odontolyticus* causes non-attachment pathogenesis, we performed a Transwell co-culture assay, in which iCECs were co-cultured without direct attachment of bacteria due to the separation with a 0.4 μm filter (Figure 2*B*). In this assay, NF-κB signaling in iCECs was significantly activated at 6 hours after adding *A odontolyticus,* and a more significant increase was observed at 24 hours (Figure 2*C*). These results suggested that *A odontolyticus* secretes pathogens in the culture supernatant, which may activate NF-κB signaling in iCECs without direct attachment.

The release of EVs are universal features of all living cells including bacteria.[19] Whereas EVs released from Gram-negative bacteria are called outer membrane vesicles (OMVs), EVs from Gram-positive bacteria are called as MVs.[20] Although biological functions of MVs released from some specific Gram-positive bacteria have been examined,[21,22] it was unknown whether *A odontolyticus* also secretes MVs. We hypothesized that *A odontolyticus* secretes MVs, which communicate with host cells, executing virulence. To examine this, we tried to determine MVs from culture media incubating *A odontolyticus* by ultracentrifugation and size exclusion chromatography. The extracted *A odontolyticus* MVs (A.o MVs) were visualized by transmission electron micrography, which revealed spherical vesicles. The ultrathin section of the pellet embedded in the epoxy resin suggested that MVs were released from *A odontolyticus* because the characteristic spherical structure with approximately 120 nm in diameter is contacted with the surface of the bacteria (Figure 2*D* and *E*). A.o MVs were detected as white dots using NanoSight LM10 but were not observed in extracts from medium alone (Figure 2*F*). Nitrate reductase and DNA-directed RNA polymerase subunit beta (approximately 140 kDa) and enolase and dihydrolipoyl dehydrogenase (approximately 45 kDa) were identified in A.o MVs, determined by liquid chromatography-mass spectrometry (Figure 2*G*), suggesting that intracellular and plasma membrane enzymes exist in A.o MVs.

Next, we examined whether A. oMVs activate NF-κB signaling in iCECs. NF-κB–driven luciferase levels were increased by the treatment of A.o MVs, which were suppressed by NF-κB inhibitors BAY11-7082 or JSH23 (Figure 2*H*). A dose-dependent increase in IL 8 and TNFα mRNA levels was detected by the treatment of A.o MVs (Figure 2*I*).

Toll-like Receptor 2 Is Responsible for Inducing Proinflammatory Signaling by A.o MVs

Bacterial pathogen-associated molecular patterns such as membrane lipoproteins, lipopolysaccharides, lipoteichoic acid (LTA), and peptidoglycans are well-known to modulate host immune responses by activating toll-like receptor (TLR) signaling pathways.[23] To test which receptor was activated by A.o MVs, we performed quantitative reverse transcription-polymerase chain reaction using TLR2$^{-/-}$, TLR4$^{-/-}$, TLR9$^{-/-}$, TLR2/4/9 triple knockout, or MYD88$^{-/-}$ mouse embryo fibroblasts. In wild-type cells, TLR4$^{-/-}$ and TLR9$^{-/-}$ cells treated with A.o MVs mRNA levels of IL-6 and TNFα were increased. In contrast, in TLR2$^{-/-}$, TLR2/4/9 triple knockout, and MYD88$^{-/-}$ cells those mRNA levels were not increased, suggesting that TLR2 is responsible for the proinflammatory signaling induction by A.o MVs (Figure 3*A*). To examine these in human cells, we generated

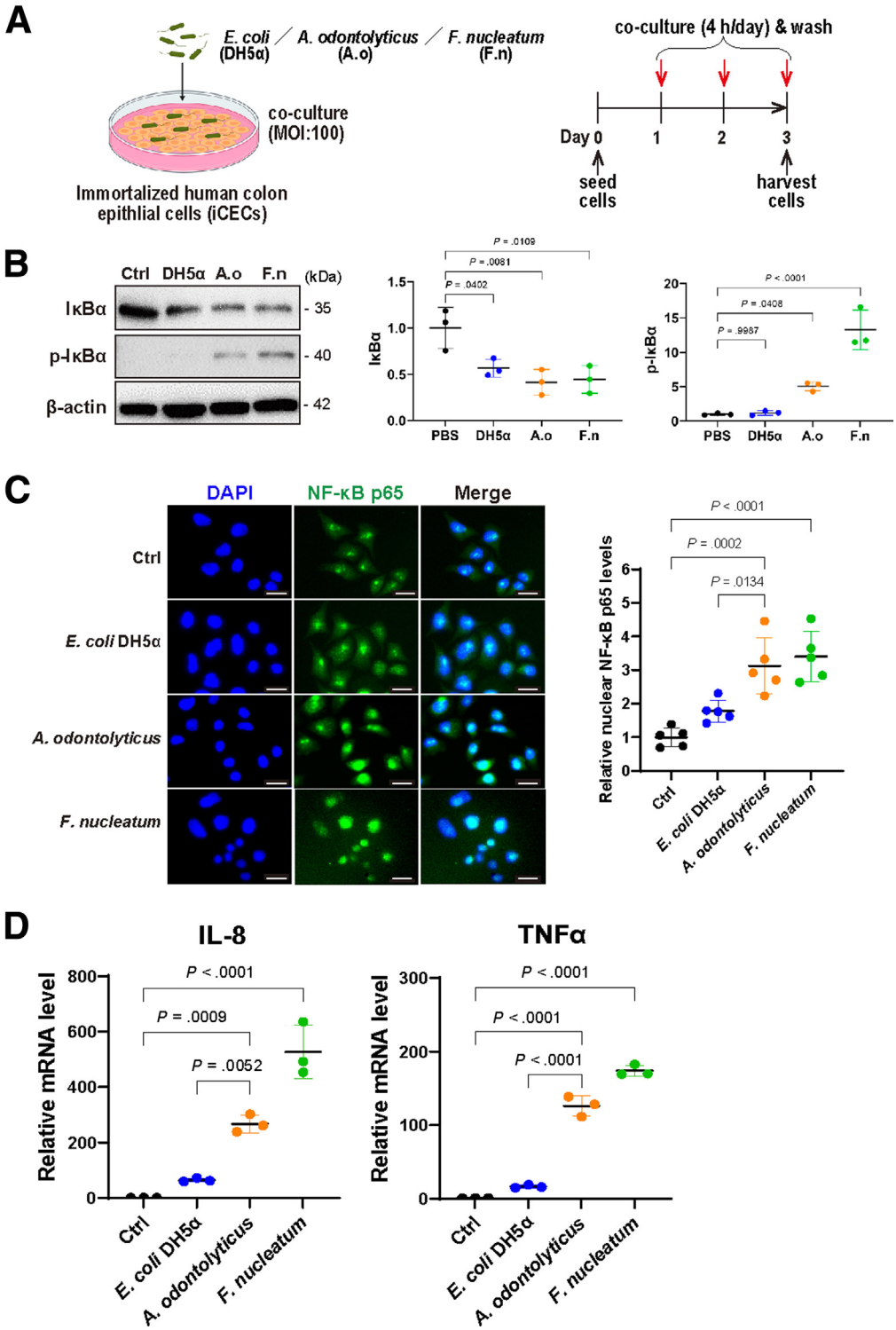

Figure 1. NF-κB signaling is activated by *A odontolyticus*. (*A*) Scheme and time course of co-culture. iCECs were exposed to bacteria (multiplicity of infection = 100) for 4 h/day. This procedure was repeated for 3 consecutive days. (*B*) Representative Western blots of inhibitor of κBα (IκBα) and phosphorylation levels of IκBα (p-IκBα) of iCECs co-cultured with *A odontolyticus* (A.o) at day 3, compared with PBS, *E coli* (DH5α), and *F. nucleatum* (F.n) (n = 3). Relative band intensities normalized to β-actin. Data are shown as mean ± SD of 3 technical replicates (n = 3). (*C*) Representative immunofluorescence images of nuclear translocation of NF-κB subunit p65 (*green*) in iCECs co-cultured with bacteria at day 3 are shown in *left panels* (n = 5). Cell nuclei were counterstained with DAPI (*blue*). Scale bars represent 20 μm. Quantitated relative nuclear transfer levels of NF-κB p65 are shown in *right panel*. Data are shown as mean ± SD of 3 technical replicates (n = 5). (*D*) Quantitative reverse transcription-polymerase chain reaction analyses of IL-8 and TNFα levels in iCECs co-cultured with bacteria at day 3. Data are shown as mean ± SD of 3 technical replicates (n = 3). *P* values calculated using one-way ANOVA followed by Tukey's test.

human iCECs with TLR2 or MYD88 knockout using the CRISPR-Cas9 system (Figure 3*B*), and similar results were observed (Figure 3*C*).

Because *A odontolyticus* is a Gram-positive bacterium, peptidoglycans and LTA exist in those outer surfaces, known as ligands for TLR2.[24] We further determined whether A.o MVs also have these cell wall components. Although A.o MVs have less peptidoglycans levels than whole cell lysate or soluble membrane protein of *A odontolyticus*, they have clearly more LTA levels (Figure 3*D* and *E*). In iCECs treated with MVs, IL-8 and TNFα mRNA levels were significantly increased, compared with those when

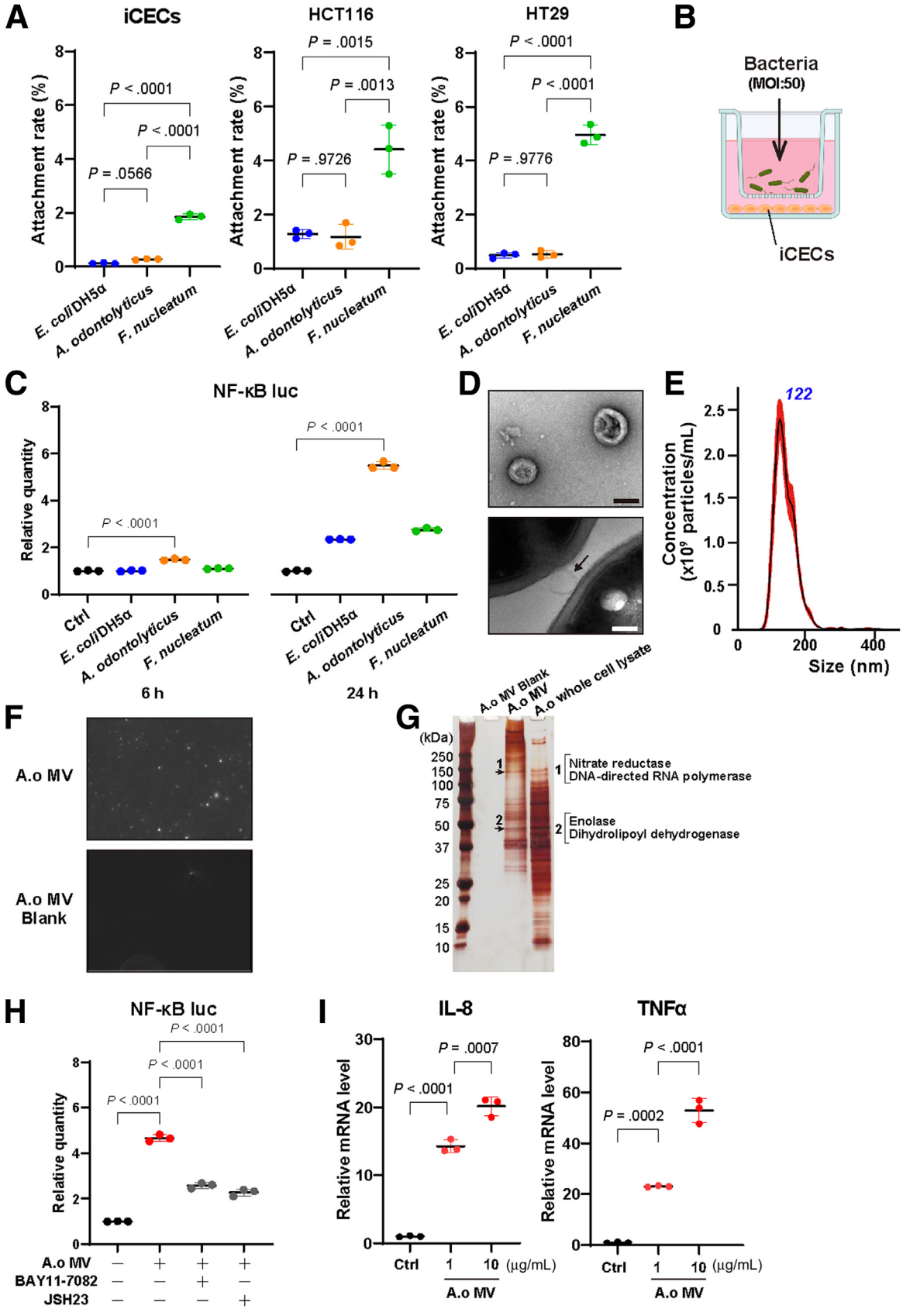
A
iCECs
HCT116
HT29
Attachment rate (%)
P < .0001
P < .0001
P = .0566
P = .0015
P = .0013
P = .9726
P < .0001
P < .0001
P = .9776
E. coliDH5α
A. odontolyticus
F. nucleatum
B
Bacteria
(MOI:50)
iCECs
C
NF-κB luc
Relative quantity
P < .0001
P < .0001
Ctrl
E. coliDH5α
A. odontolyticus
F. nucleatum
6 h
24 h
D
E
122
Concentration
(x10⁹ particles/mL)
Size (nm)
F
A.o MV
A.o MV
Blank
G
A.o MV Blank
A.o MV
A.o whole cell lysate
(kDa)
250
150
100
75
50
37
25
20
15
10
1
2
1 Nitrate reductase
DNA-directed RNA polymerase
2 Enolase
Dihydrolipoyl dehydrogenase
H
NF-κB luc
Relative quantity
P < .0001
P < .0001
P < .0001
A.o MV
BAY11-7082
JSH23
I
IL-8
TNFα
Relative mRNA level
P = .0007
P < .0001
P < .0001
P = .0002
Ctrl
1
10 (μg/mL)
A.o MV

using whole cell lysate or membrane protein (Figure 3*F*). Furthermore, these cytokine levels were decreased when LTA was deacylated by platelet-activating factor–acetylhydrolase or degraded by NaOH hydrolysis treatment (Figure 3*G*). These results suggest that the LTAs of A.o MVs promote proinflammatory signaling via TLR2 in colonic epithelial cells.

A.o MVs Increase Reactive Oxygen Species Levels in Colon Epithelial Cells

Activation of TLR-related pathway and NF-κB pathway by bacteria such as *Peptostreptococcus anaerobius*[25] and a *Bacteroides fragilis* toxin leads to up-regulation of intracellular reactive oxygen species (ROS) levels and DNA damages,[26] resulting in colonic tumorigenesis. Here we hypothesized that activated NF-κB signaling through TLR2 by A.o MVs is involved in the overproduction of ROS and the induction of DNA damages. To test this hypothesis, we first examined whether intracellular ROS levels were increased by *A odontolyticus.* Indeed, ROS levels in iCECs co-cultured with *A odontolyticus* were significantly increased over time, compared with those when co-cultured with *E coli* or *F nucleatum* (Figure 4*A*), whereas ROS levels were partially increased at day 2 when cells were co-cultured with *F nucleatum,* consistent with a previous report.[27]

Next, we examined whether A.o MVs increase the ROS levels, compared with MVs from *Lacticaseibacillus rhamnosus*,[22] Gram-positive bacterium as a control. The size distribution of MVs from *L rhamnosus* was comparable with those of A.o MVs[22] (Figure 4*B*). *L rhamnosus* MVs contained LTA at a similar level to that of A.o MVs (Figure 4*C*). ROS induction levels in iCECs were significantly more by A.o MVs, compared with those by *L rhamnosus* MVs (Figure 4*D*). Elevated levels of γH2AX, a marker of double-stranded DNA breaks, and p21, a key mediator of cell cycle arrest in response to DNA damages, showed the subsequent induction of DNA damages by A.o MVs (Figure 4*E*). These up-regulations were inhibited by N-acetyl-L-cysteine, a scavenger of ROS, suggesting that the DNA damages were induced via ROS production by A.o MVs (Figure 4*E*). Consistently, γH2AX positive iCECs were markedly increased by A.o MVs (Figure 4*F*). These effects were induced more by A.o MVs than by *L rhamnosus* MVs (Figure 4*E* and *F*). G_2/M-phase cells and fewer S-phase cells were observed when iCECs were treated with A.o MVs for 48 hours than control cells (Figure 4*G*). Furthermore, we performed a transcriptomic analysis of iCECs treated with A.o MVs compared with the PBS control. Results revealed the most differentially enriched pathways, as identified by gene set enrichment analysis (Figure 4*H*). Consistently, a marked increase was observed in the expression levels of cell cycle-regulated genes, such as those in the E2F, G2M checkpoint, and p53 pathways (Figure 4*I*).

Next, we examined the effects of A.o MVs in human tissues using a gut organoid, derived normal human induced pluripotent stem cells (iPSCs). To examine the effects of A.o MVs from the luminal side of the gut organoid, we used a specific gut organoid with apical-out, which is different from conventional ones, making it possible to treat the epithelial cells from outside of the organoid (Figure 5*A*). The localization of villin in the surface of the organoids as a marker for the brush border of the colonic epithelia was confirmed (Figure 5*B*). Differentiated Paneth cells or endocrine cells were also confirmed by lysozyme or chromogranin A staining, respectively (Figure 5*B*). In addition, the expression of caudal type homeobox 2, mucin2, and cadhelin-17 as epithelial cell markers and alpha smooth muscle actin as the smooth muscle cell marker were also confirmed as expected (Figure 5*C*). Consistent with the results obtained using cell lines, A.o MVs–induced double-stranded DNA breaks in the epithelial cells of the human gut-mimic model were more than those induced by *L rhamnosus* MVs (Figure 5*D*).

A.o MVs Induced Cellular Transformation in Vitro and Colorectal Dysplasia in Mice

To determine whether A.o MVs can induce cellular transformation via induction of DNA damages, we performed a colony formation assay using iCECs. Cells were treated with A.o MVs every 3 days and split every 6 days for 3 months, followed by seeding the cells on soft agar plates,

Figure 2. (***See previous page***). ***A odontolyticus*** **releases membrane vesicles.** (*A*) Attachment levels of *A odontolyticus* on iCECs, HCT116, and HT29, compared with DH5α and *F nucleatum*. Data are shown as mean ± SD of 3 technical replicates (n = 3). *P* values were calculated using one-way ANOVA followed by Tukey's test. (*B*) An illustration of the Transwell co-culture assay is shown. Bacteria and iCECs were cultured in the upper and the bottom chambers, respectively. (*C*) Relative luciferase levels from NF-κB–driven luciferase construct at 6 and 24 hours after seeding bacteria are shown. PBS was used as a negative control. Data are shown as mean ± SD of 3 technical replicates (n = 3). *P* values calculated using one-way ANOVA followed by Tukey's test. (*D*) Transmission electron micrograph of A.o MVs. Negative staining of A.o MVs is shown in *upper panel*. Ultrathin section of *A odontolyticus* pellet is shown in *lower panel*. *Arrow* indicates the released MV from the bacteria. Scale bar represents 100 nm. (*E*) Size distribution of A.o MVs isolated from culture supernatant of *A odontolyticus*, analyzed by the nanoparticles tracking analysis. (*F*) MVs extracted from supernatant of liquid broth cultured with *A odontolyticus* were observed as *white dots* by the NanoSight microscopy. Those dots were not observed in the broth without bacterial culture. (*G*) Silver-staining images of A.o MVs and bacterial lysates after SDS-polyacrylamide gel electrophoresis. Representative bands in A.o MVs and in bacterial lysates observed were analyzed by liquid chromatography–mass spectrometry. Proteins identified from each band are indicated. (*H*) Relative luciferase levels from NF-κB–driven luciferase construct at 24 hours after treatment of A.o MVs (10 μg/mL) with or without NF-κB inhibitor BAY11-7082 or JSH23 (n = 3). PBS was used as a negative control. Data are shown as mean ± SD of 3 technical replicates (n = 3). *P* values were calculated using one-way ANOVA followed by Tukey's test. (*I*) Quantitative reverse transcription-polymerase chain analyses of IL-8 and TNFα mRNA levels after 24 hours of A.o MVs treatments (1, 10 μg/mL) in iCECs. Data are shown as mean ± SD of 3 technical replicates (n = 3). *P* values calculated using one-way ANOVA followed by Tukey's test.

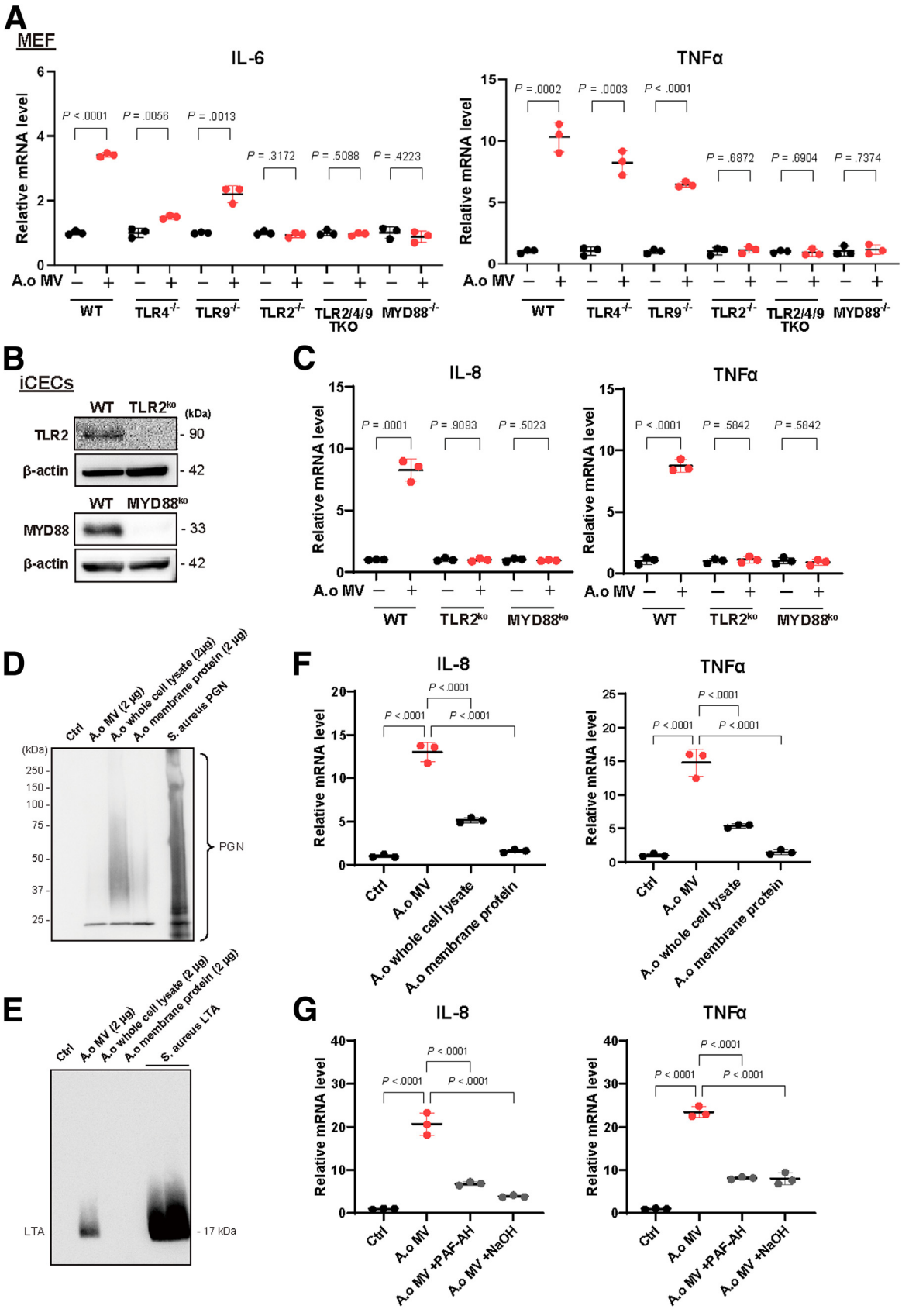
A
MEF
IL-6
TNFα
Relative mRNA level
P < .0001
P = .0056
P = .0013
P = .3172
P = .5088
P = .4223
P = .0002
P = .0003
P < .0001
P = .6872
P = .6904
P = .7374
A.o MV
WT
TLR4-/-
TLR9-/-
TLR2-/-
TLR2/4/9 TKO
MYD88-/-
B
iCECs
WT
TLR2ko
(kDa)
TLR2
β-actin
- 90
- 42
MYD88ko
MYD88
- 33
C
IL-8
TNFα
P = .0001
P = .9093
P = .5023
P < .0001
P = .5842
P = .5842
TLR2ko
MYD88ko
D
Ctrl
A.o MV (2 μg)
A.o whole cell lysate (2μg)
A.o membrane protein (2 μg)
S. aureus PGN
(kDa)
250
150
100
75
50
37
25
PGN
E
S. aureus LTA
LTA
- 17 kDa
F
IL-8
TNFα
P < .0001
A.o whole cell lysate
A.o membrane protein
G
IL-8
TNFα
A.o MV +PAF-AH
A.o MV +NaOH

and the cells were cultured for 2 weeks (Figure 6*A*). The treatment with A.o MVs resulted in a significant increase in the number of colonies, suggesting that the colon epithelial cells treated with A.o MVs were susceptible to cellular transformation (Figure 6*B*).

To examine in vivo the potential of the induction of cellular transformation in colon epithelia by A.o MVs, A.o MVs or vehicle PBS were injected once a week via the transanal route into BALB/c mice (Figure 6*C*). After 2 months of treatment, A.o MVs–treated mice showed a significant increase in γH2AX-positive colon epithelial cells (Figure 6*D*). Furthermore, the A.o MVs–treated mice showed dysplastic lesions in the distal colon epithelia (Figure 6*E*). These results suggest that A.o MVs are mutagenic and induce dysplasia in the colon.

A.o MVs Are Internalized by the Host Cells, Leading to ROS Overproduction

On the basis of the findings that A.o MVs induce DNA damages in the colon cells and dysplasia, we examined the underlying mechanisms further. Because A.o MVs promoted the NF-κB pathway through TLR2, we suspected that these pathways were involved in the ROS production and subsequent induction of DNA damages. However, high ROS production levels by A.o MVs remained in TLR2 knockout iCECs (Figure 7*A*) as well as when using NF-κB inhibitors (Figure 7*B*). These results suggest that another mechanism, apart from the TLR2–NF-κB pathway, exists in the ROS production in iCECs by A.o MVs.

Some bacterial MVs are internalized into host cells and exert biological effects in the cells.[20] These findings led us to hypothesize that the internalization of A.o MVs into host cells is involved in ROS overproduction in colon epithelial cells. To test whether A.o MVs are internalized into host cells, we examined iCECs, to which the fluorescently labeled-A.o MVs were added using fluorescent microscopy. Although A.o MVs were internalized into iCECs at 37°C, such internalization was inhibited at 4°C, suggesting that the process was mediated by endocytosis (Figure 7*C*). TLR2 was not involved in this internalization because A.o MVs were internalized similarly into $TLR2^{ko}$ and WT cells (Figure 7*D*). To determine the related endocytosis in more detail, we performed a fluorescent assay using different types of endocytosis inhibitors. After determining the appropriate concentration of each inhibitor by cytotoxicity tests (Figure 7*E*), iCECs were pre-incubated with control (dimethyl sulfoxide), Dynasore, Dyngo 4a, Filipin III, Chlorpromazine, Cytochalasin D, or Nocodazole for 1 hour, followed by adding the fluorescently labeled A.o MVs. Among them, Dynasore and Dyngo 4a, dynamin (DNM) inhibitors, significantly blocked the internalization of A.o MVs into iCECs (Figure 7*F*). Furthermore, Dynasore and Dyngo 4a significantly suppressed the ROS overproduction in iCECs induced by A.o MVs (Figure 7*G*).

In addition, we evaluated cells with DNM knocked down to assess the off-target effects of these inhibitors. DNMs, guanosine triphosphatases associated with endocytosis, are categorized into 3 types: DNM1, DNM2, and DNM3.[28] Quantitative polymerase chain reaction results revealed that iCECs predominantly expressed DNM1 and DNM2, not DNM3 (Figure 7*H*). We then used siRNA to create cells with either DNM1 or DNM2 knocked down (Figure 7*H*). As expected, the overproduction of ROS induced by A.o MVs was significantly reduced in cells with DNM1 or DNM2 knocked down (Figure 7*I*). Next, considering that CpG motifs in bacterial DNA, which interact with TLR9, reportedly cause pH-dependent ROS generation,[29] we investigated whether these processes are affected by the inhibitors of endosomal maturation and acidification, ie, bafilomycin A, monensin, and chloroquine. Optimal concentrations for these agents are presented in Figure 7*J*. However, the tested concentrations of these inhibitors did not suppress the ROS overproduction induced by A.o MVs (Figure 7*K*).

These results suggest that ROS overproduction in iCECs by A.o MVs is mediated through the internalization of A.o MVs into host cells via DNM-dependent endocytosis other than clathrin-mediated endocytosis.

Internalized A.o MVs Are Co-localized With Mitochondria and Disrupt Their Function

Furthermore, we tried to determine the mechanisms bridging the A.o MVs internalization and ROS overproduction in CECs. Because it is known that mitochondria are important sources of ROS in mammalian cells and mitochondrial dysfunction leads to ROS overproduction,[30] we hypothesized that ROS overproduction by A.o MVs was caused by host mitochondrial dysfunction. To confirm that

Figure 3. (***See previous page***). **TLR2 plays a key role in proinflammatory signaling induced by A.o MVs.** (*A*) Quantitative reverse transcription-polymerase reaction chain analyses of IL-6 and TNFα levels in wild-type (WT), $TLR4^{-/-}$, $TLR9^{-/-}$, $TLR2^{-/-}$, TLR2/4/ 9 triple-KO (TKO), or $MYD88^{-/-}$ mouse embryonic fibroblasts (MEFs) after 24 hours of A.o MVs (1 μg/mL) treatment (n = 3). Data are shown as mean ± SD of 3 technical replicates (n = 3). *P* values were calculated using the 2-sided Welch *t* test. (*B*) Confirmation of knockout of TLR2 or MYD88 in iCECs by Western blotting. (*C*) Quantitative reverse transcription-polymerase chain reaction analyses of IL-6 and TNFα levels in WT, TLR2 knockout ($TLR2^{ko}$), or MYD88 knockout ($MYD88^{ko}$) iCECs after 24 hour of A.o MVs (1 μg/mL) treatment. Data are shown as mean ± SD of 3 technical replicates (n = 3). *P* values were calculated using the 2-sided Welch *t* test. (*D*) Western blotting results of peptidoglycans (PGN) from 2 μg of A.o MVs, A.o whole cell lysate (WC), or A.o membrane proteins (MP) are shown. PGN (20 μg) from *Staphylococcus aureus (S aureus)* was used as a positive control. (*E*) Western blotting results of LTA from 2 μg of A.o MVs, WC, and MP are shown. A.o MVs contain more LTA levels than WC or MP. LTA (20 and 40 μg) from *S aureus* was used as positive controls. (*F*) Quantitative reverse transcription-polymerase chain reaction analyses of IL-8 and TNFα mRNA levels after 24 hours of A.o MVs, WC, MP treatments (1 μg/mL) in iCECs. Data are shown as mean ± SD of 3 technical replicates (n = 3). *P* values calculated using one-way ANOVA followed by Tukey's test. (*G*) Quantitative reverse transcription-polymerase chain reaction analysis of IL-8 and TNFα mRNA levels after 24 hours of treatment with LTA-inactivated A.o MVs. Data are shown as mean ± SD of 3 technical replicates (n = 3). *P* values calculated using one-way ANOVA followed by Tukey's test.

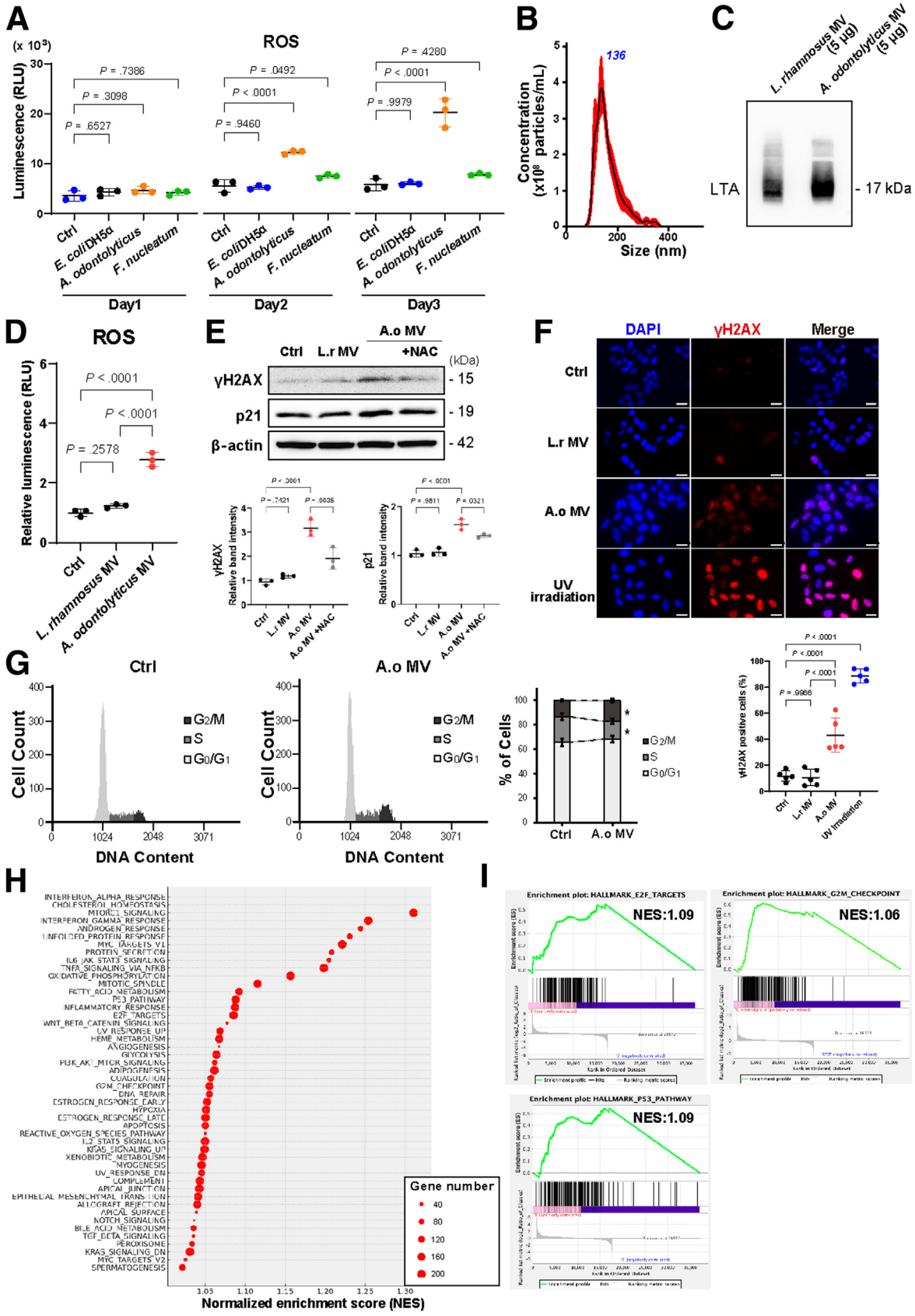
A
ROS
(x 10³)
Luminescence (RLU)
P = .7386
P = .3098
P = .6527
P = .0492
P < .0001
P = .9460
P = .4280
P < .0001
P = .9979
Ctrl
E. coliDH5α
A. odontolyticus
F. nucleatum
Day1
Day2
Day3
B
136
Concentration (x10⁸ particles/mL)
Size (nm)
C
L. rhamnosus MV (5 μg)
A. odontolyticus MV (5 μg)
LTA
- 17 kDa
D
ROS
Relative luminescence (RLU)
P < .0001
P < .0001
P = .2578
Ctrl
L. rhamnosus MV
A. odontolyticus MV
E
A.o MV
Ctrl
L.r MV
+NAC
(kDa)
γH2AX
p21
β-actin
- 15
- 19
- 42
Relative band intensity
P = .7421
P = .0035
P = .9811
P = .0321
Ctrl
L.r MV
A.o MV
A.o MV +NAC
F
DAPI
γH2AX
Merge
Ctrl
L.r MV
A.o MV
UV irradiation
G
Ctrl
A.o MV
Cell Count
G2/M
S
G0/G1
DNA Content
% of Cells
P < .0001
P < .0001
P < .0001
P = .9966
γH2AX positive cells (%)
UV irradiation
H
INTERFERON_ALPHA_RESPONSE
CHOLESTEROL_HOMEOSTASIS
MTORC1_SIGNALING
INTERFERON_GAMMA_RESPONSE
ANDROGEN_RESPONSE
UNFOLDED_PROTEIN_RESPONSE
MYC_TARGETS_V1
PROTEIN_SECRETION
IL6_JAK_STAT3_SIGNALING
TNFA_SIGNALING_VIA_NFKB
OXIDATIVE_PHOSPHORYLATION
MITOTIC_SPINDLE
FATTY_ACID_METABOLISM
P53_PATHWAY
INFLAMMATORY_RESPONSE
E2F_TARGETS
WNT_BETA_CATENIN_SIGNALING
UV_RESPONSE_UP
HEME_METABOLISM
ANGIOGENESIS
GLYCOLYSIS
PI3K_AKT_MTOR_SIGNALING
ADIPOGENESIS
COAGULATION
G2M_CHECKPOINT
DNA_REPAIR
ESTROGEN_RESPONSE_EARLY
HYPOXIA
ESTROGEN_RESPONSE_LATE
APOPTOSIS
REACTIVE_OXYGEN_SPECIES_PATHWAY
IL2_STAT5_SIGNALING
KRAS_SIGNALING_UP
XENOBIOTIC_METABOLISM
MYOGENESIS
UV_RESPONSE_DN
COMPLEMENT
APICAL_JUNCTION
EPITHELIAL_MESENCHYMAL_TRANSITION
ALLOGRAFT_REJECTION
APICAL_SURFACE
NOTCH_SIGNALING
BILE_ACID_METABOLISM
TGF_BETA_SIGNALING
PEROXISOME
KRAS_SIGNALING_DN
MYC_TARGETS_V2
SPERMATOGENESIS
Gene number
Normalized enrichment score (NES)
I
Enrichment plot: HALLMARK_E2F_TARGETS
NES:1.09
Enrichment plot: HALLMARK_G2M_CHECKPOINT
NES:1.06
Enrichment plot: HALLMARK_P53_PATHWAY
NES:1.09

the ROS overproduction by the treatment of A.o MVs is of mitochondrial origin, we performed fluorescence analyses using Mito-SOX, which stains mitochondrial superoxide generation. The number of Mito-SOX–stained cells increased after treatment with A.o MVs compared with those after treatment with *L rhamnosus* MVs (Figure 8*A*). Furthermore, treatment with A.o MVs resulted in significant reduction in mitochondrial DNA (mtDNA) copy number, which was effectively suppressed by Dynasore (Figure 8*B*). This suggested that the endocytosis of A.o MVs into cells induces mitochondrial dysfunction. This result was supported by the increased fragmentation of the mitochondrial networks, a recognized indicator of mitochondrial dysfunction, which is typically associated with impaired respiration and oxidative phosphorylation (OXPHOS),[31] in iCECs after treatment with A.o MVs (Figure 8*C*). Immunofluorescence staining for TOMM20, a marker of the mitochondrial outer membrane, showed similar fragmentation patterns after exposure to A.o MVs (Figure 8*D*). Notably, the reduction in mtDNA copy number decreased the transcriptional levels of mitochondrial electron transport chain genes,[32] as shown by down-regulation of NDUFB8 (Complex I), SDHB (Complex II), and COX II (Complex IV) proteins in response to A.o MV treatment (Figure 8*E*). Moreover, the mitochondrial respiratory function, which is measured by the oxygen consumption rate (OCR), was significantly decreased after 4 hour and 48 hours after treatment with A.o MVs (Figure 8*F*). Glycolysis levels, which are indicated by the extracellular acidification rate, showed a tendency toward elevation. This suggested the initiation of metabolic switching. However, the difference was not statistically significant (Figure 8*G*). To investigate the effect of A.o MVs on mitochondria in more detail, we examined the co-localization of A.o MVs and mitochondria using an immunofluorescence assay, which revealed that the labeled A.o MVs co-localize with mitochondria (Figure 8*H*). To assess the binding of A.o MVs to the mitochondrial outer membrane in vitro, we performed an immunoprecipitation assay. To this end, we mixed A.o MVs with mitochondria, which were extracted while maintaining their intact state, and immunoprecipitated using TOMM20, a mitochondrial outer membrane protein. Results showed that LTA, a component of A.o MVs, co-precipitated with TOMM20 (Figure 8*I*). Thus, these results strongly indicate that internalized A.o MVs can disrupt mitochondrial function and induce excessive ROS production.

Taken together, our results showed that MVs produced from *A odontolyticus* not only induce inflammation but also cause mitochondrial dysfunction and DNA damages via internalization and subsequent mitochondrial co-localization in the CECs. These results suggested that the internalized A.o MVs co-localize with mitochondria, leading to mitochondrial dysfunction and ROS overproduction.

Discussion

Recent advances in metagenomic analyses have revealed that *A odontolyticus* is particularly abundant in the early stages of CRC.[11] However, its biological function in the process of colorectal carcinogenesis remains unknown. We showed that *A odontolyticus* produces MVs, which induce not only inflammation but also excessive ROS production via mitochondrial dysfunction, leading to DNA damages and intestinal dysplasia. Our results provide new insights into the pathogenesis of colorectal tumorigenesis at the early stages by *A odontolyticus*–derived MVs.

Although *A odontolyticus* is a pathogen of thoracic and abdominal actinomycosis,[12] *A odontolyticus* is a major member of bacteria existing in the oral cavity, similar to *F nucleatum,*[13] which is also associated with the pathogenesis of CRC. In the case of *F nucleatum,* bacterial attachment to the host cells is the first step in tumorigenesis, similar to the cases of *P anaerobius* and *Bacteroides fragilis*.[17,33,34] However, we found that *A odontolyticus* has only a low adhesion level to the host cells, and instead, it secretes MVs, which are pathogenic to colon cells. Although some intestinal bacteria microbiotas are known to secrete MVs that have biological

Figure 4. (***See previous page***). **Induction of ROS by A.o MVs.** (*A*) iCECs were co-cultured with *E coli* DH5α, *A odontolyticus*, and *F nucleatum* (multiplicity of infection = 100) for 4 h/day. PBS was used as a control. ROS levels in iCECs on days 1, 2, and 3 are shown. Data are shown as mean ± SD of 3 biological replicates (n = 3). *P* values were calculated using one-way ANOVA followed by Tukey's test. (*B*) Size distribution of MVs from *L rhamnosus* analyzed by nanoparticles tracking analysis. (*C*) Western blotting results of LTA from *L rhamnosus* MVs (5 μg) and A.o MVs (5 μg). (*D*) Relative ROS levels in iCECs at 24 hours after treatment with PBS or MVs (20 μg/mL) from *A odontolyticus* and *L rhamnosus*. Data are shown as mean ± SD of 3 biological replicates (n = 3). *P* values calculated using one-way ANOVA followed by Tukey's test. (*E*) Representative results of Western blots showing γH2AX and p21 levels in iCECs at 48 hours after treatment with PBS, *L rhamnosus* MVs, or A.o MVs (20 μg/mL), with or without 5 mmol/L of N-acetyl-L-cysteine, a ROS scavenger. Relative band intensities normalized to β-actin are shown in *lower panel*. Data are shown as mean ± SD of 3 technical replicates (n = 3). (*F*) Representative immunofluorescence images of γH2AX (*red*) in iCECs at 24 hours after treatment with PBS, *L rhamnosus* MVs, or A.o MVs (20 μg/mL). For the positive control of the double-stranded DNA breaks, cells at 24 hours after UV irradiation were used. DAPI (*blue*) indicates nuclei. Scale bars represent 20 μm. Rates of γH2AX-positive cells were calculated (*lower panel*). Data are shown as mean ± SD of 3 technical replicates (n = 5). *P* values were calculated using one-way ANOVA followed by Tukey's test. (*G*) Representative results about cell cycle analysis of iCECs at 48 hours after A.o MVs treatment (20 μg/mL) (*left 2 panels*). *Bar graph* obtained from cell cycle analysis showing percentage of cells in different phases of the cell cycle (G_2/M, S, and G_0/G_1) in the *right panel*. Data are shown as mean ± SD of 3 technical replicates (n = 3). *$P < .05$, 2-sided Welch *t* test. (*H*) Scatter plot of gene set enrichment analysis (GSEA) using MSigDB Hallmark gene sets (version 4.2.1) showing significantly differentially regulated pathways in iCECs treated with A.o MVs compared with PBS controls; false discovery ratio (FDR) < .25. (*I*) Enrichment plot showing up-regulation of E2F targets, G2M checkpoint, and p53 pathway in iCECs treated with A.o MVs compared with PBS control. NES, normalized enrichment score.

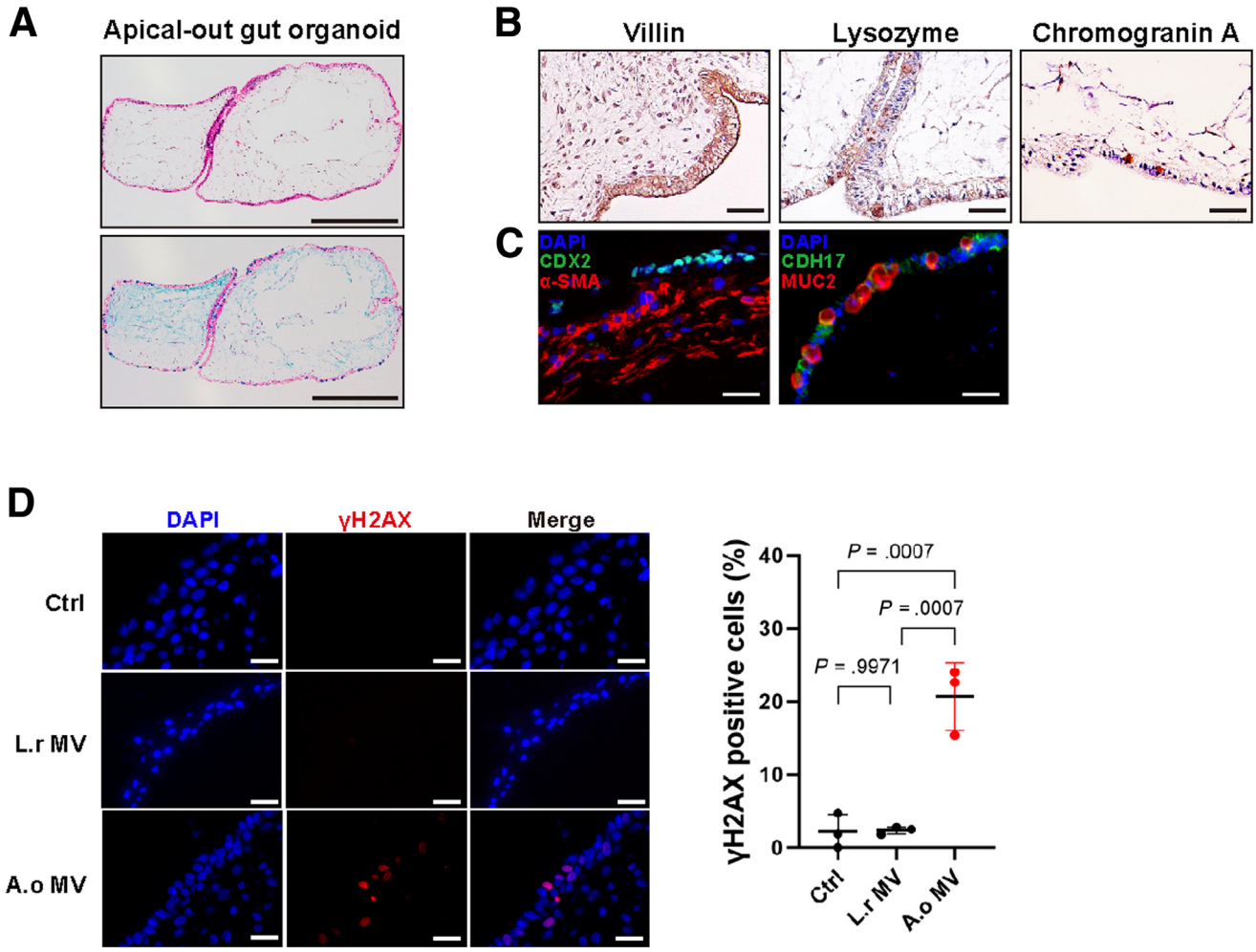

Figure 5. A.o MVs induced DSBs in human gut-mimic model. (*A*) Apical-out human gut organoids are generated from induced pluripotent stem cells (iPS cells). H&E and alcian blue staining images of the organoid are shown. Scale bars represent 500 μm. (*B* and *C*) Immunohistochemistry staining villin, lysozyme, and chromogranin A in the human gut organoids are shown in the upper. Immunofluorescence images of caudal type homeobox 2 (CDX2), alpha-smooth muscle actin (α-SMA), cadherin-17, and mucin 2 (MUC2) are shown in the lower. These images show the proper differentiation of the organoids. Scale bars represent 50 μm. (*D*) Representative immunofluorescence images of γH2AX in the organoids at 1 week after treatment with PBS, *L rhamnosus* MVs, or A.o MVs (20 μg/mL). Scale bars represent 20 μm. Right: γH2AX-positive cell ratios. Data are shown as mean $\pm$ SD of 3 technical replicates (n = 3). *P* values were calculated using one-way ANOVA followed by Tukey's test.

functions, to our best knowledge, there have been no reports of MVs secreted by *A odontolyticus*, and this study is the first step showing their important biological functions.[4]

In this study, A.o MVs increased NF-κB signaling levels. NF-κB signaling is an important factor in chronic inflammation and tumorigenesis.[35,36] In fact, *F nucleatum* is known to up-regulate microRNA-21 levels and promote tumorigenesis through TLR4-mediated NF-κB signaling.[14] *P anaerobius* interacts with TLR2 and TLR4, leading to enhanced ROS production and promoting colonic tumorigenesis.[25] Although A.o MVs increased NF-κB signaling levels via TLR2, excessive ROS production was not observed in vitro. However, the possibility cannot be denied that the up-regulation of NF-κB signaling levels by A.o MVs also contributes to colonic dysplasia formation, because the chronic activation of NF-κB signaling affects tissue injury, leading to the accumulation of DNA damage.

We found that LTA in A.o MVs is responsible to activate NF-κB signaling via TLR2. Bacterial LTAs have variable structures specific to species and play important roles in bacterial homeostasis and virulence.[37] In MVs, *L rhamnosus* MVs were reported to contain LTA, which induces expression of IL-10 and has been internalized by dendritic cells.[22] Our results showed that the LTA of A.o MVs was not involved in ROS production, although A.o MVs specifically induced excessive ROS production, in contrast to the cases of *L rhamnosus* MVs. Although comprehensive views about bacterial MVs in the human colon have not been reported, the gut microbiota may secrete a variety of MVs, and the interactions with other bacterial MVs would also need to be considered.

OMVs of enterohemorrhagic *E coli* (EHEC) and *Neisseria gonorrhoeae* contain unique toxins such as EHEC hemolysin and Porin B (PorB), respectively. After these OMVs are endocytosed into host cells, the toxins target mitochondria

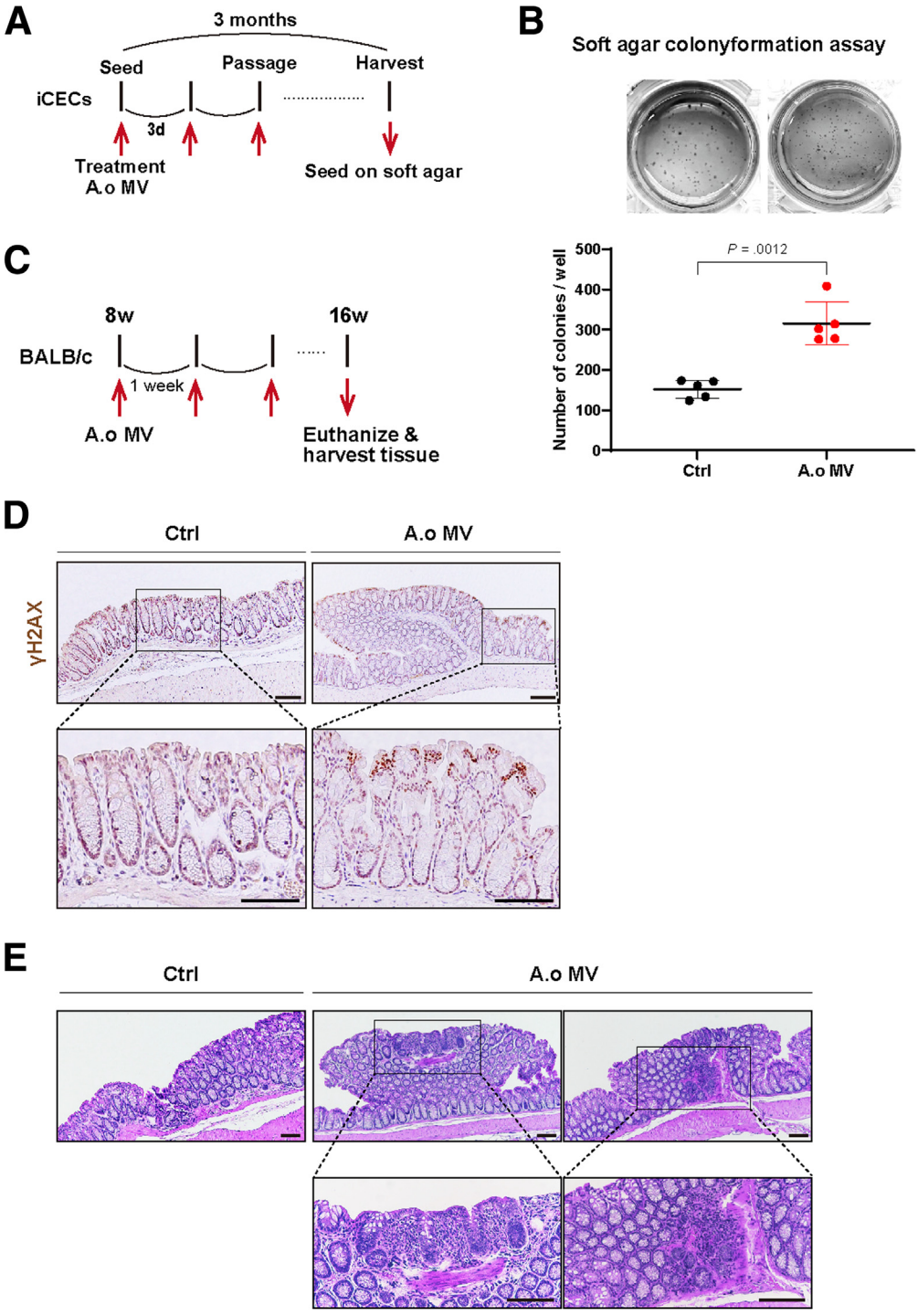

Figure 6. Effects of long treatment with A.o MVs on colonic epithelial cells in vitro and in vivo. (*A*) Experimental design of the colony formation assay using iCECs treated with A.o MVs (20 μg/mL) or same volume of PBS as a control for 3 months. (*B*) Representative images of each well are shown in *upper panels*. Number of colonies per well is shown in *lower panel*. Data are shown as mean ± SD of 3 biological replicates (n = 5). *P* values were calculated using the 2-sided Welch *t* test. (*C*) Experimental design of transanal injection of MVs to BALB/c mice. A.o MVs–treated group was injected with 20 μg of A.o MVs in 100 μL of PBS weekly for 2 months. Control group received 100 μL of PBS. (*D*) Representative immunohistochemical images of γH2AX in mice colonic epithelia. Scale bar represents 100 μm. (*E*) Representative H&E staining images of distal colonic epithelia are shown. Scale bar represents 100 μm.

and trigger the apoptotic pathway. However, it is unclear how these toxins reach mitochondria inside the recipient cells.[38,39] Similar to these cases, we found that A.o MVs are internalized by endocytosis and co-localize with mitochondria in the recipient colon cells. Bacterial toxins derived from *Helicobacter pylori* and enteropathogenic *E coli* have also been reported to target host mitochondria.[40] For example, enteropathogenic *E coli* secretes mitochondrial-associated protein, and *E coli* secreted protein F-like protein from prophage U, which have N-terminal mitochondria-targeting signal, which enter host cells[41,42] and localize to mitochondria, disrupting mitochondrial membrane potential.[43] MVs contain many proteins, lipids, nucleic acids, and other biomolecules including toxins.[44] Indeed, many proteins were observed in A.o MVs. Therefore, A.o MVs may also contain undefined factors that can target mitochondria.

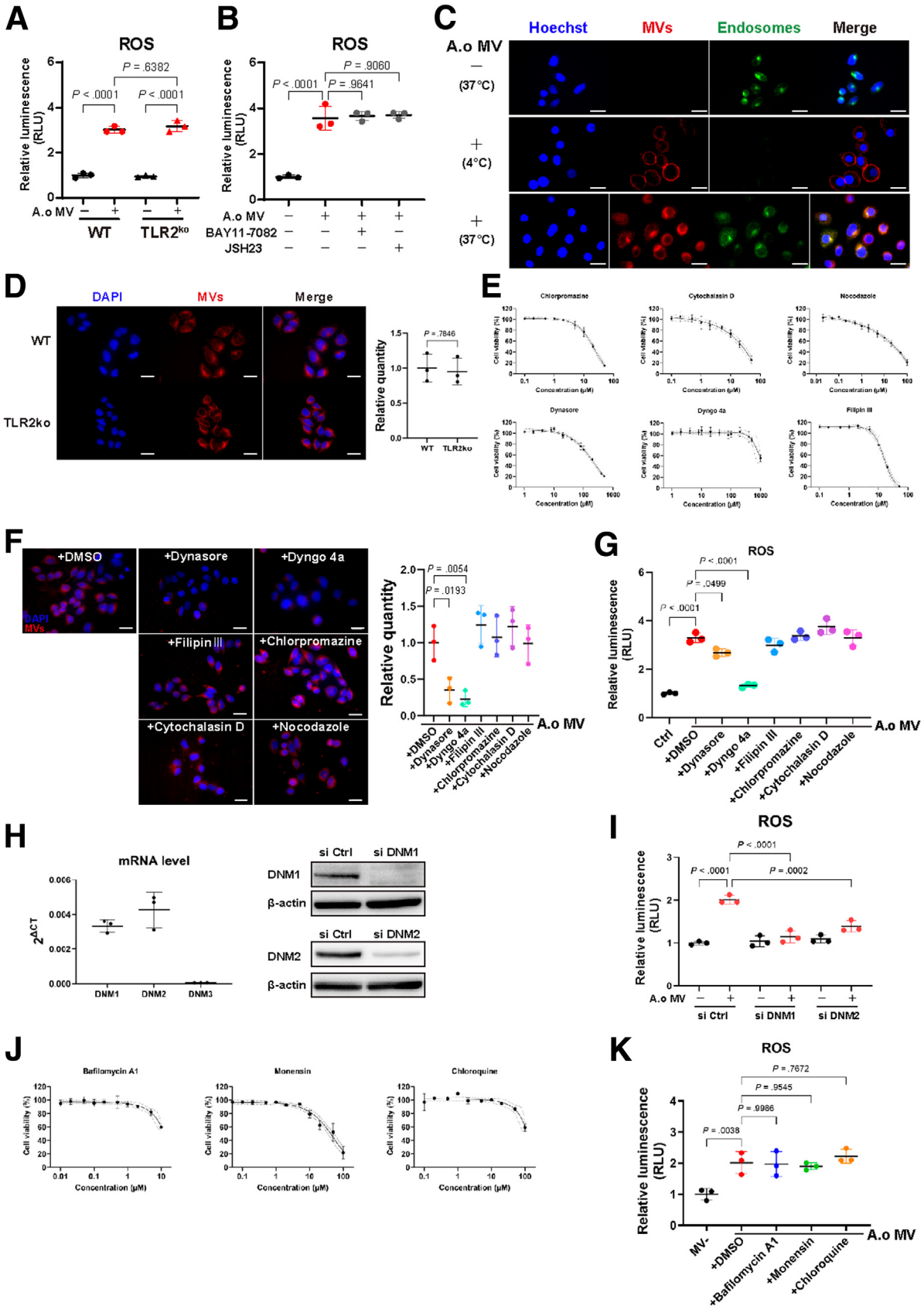
A
ROS
Relative luminescence (RLU)
P = .6382
P < .0001
P < .0001
A.o MV
WT
TLR2ko
B
ROS
Relative luminescence (RLU)
P = .9060
P < .0001
P = .9641
A.o MV
BAY11-7082
JSH23
C
Hoechst
MVs
Endosomes
Merge
A.o MV
(37°C)
(4°C)
(37°C)
D
DAPI
MVs
Merge
WT
TLR2ko
Relative quantity
P = .7846
E
Chlorpromazine
Cytochalasin D
Nocodazole
Dynasore
Dyngo 4a
Filipin III
Cell viability (%)
Concentration (μM)
F
+DMSO
+Dynasore
+Dyngo 4a
+Filipin III
+Chlorpromazine
+Cytochalasin D
+Nocodazole
DAPI
MVs
Relative quantity
P = .0054
P = .0193
A.o MV
G
ROS
Relative luminescence (RLU)
P < .0001
P = .0499
P < .0001
Ctrl
+DMSO
+Dynasore
+Dyngo 4a
+Filipin III
+Chlorpromazine
+Cytochalasin D
+Nocodazole
A.o MV
H
mRNA level
2^ΔCT
DNM1
DNM2
DNM3
si Ctrl
si DNM1
DNM1
β-actin
si Ctrl
si DNM2
DNM2
β-actin
I
ROS
Relative luminescence (RLU)
P < .0001
P < .0001
P = .0002
A.o MV
si Ctrl
si DNM1
si DNM2
J
Bafilomycin A1
Monensin
Chloroquine
Cell viability (%)
Concentration (μM)
K
ROS
Relative luminescence (RLU)
P = .7672
P = .9545
P = .9986
P = .0038
MV-
+DMSO
+Bafilomycin A1
+Monensin
+Chloroquine
A.o MV

Future studies are needed to identify the required factor in A.o MVs for the induction of mitochondrial dysfunction especially in the electron transport chain.

In the past decade, *F nucleatum* has been most studied as the colonic bacteria involved in the pathogenesis of CRC. Several therapeutic and preventive methods have been proposed based on the knowledge. For example, antibiotic metronidazole treatment reduced intratumoral *F nucleatum* burden and tumor growth.[45] Silver nanoparticles on the surface of M13 phage, which specifically binds *F nucleatum*, remodel the tumor-immune microenvironment against CRC.[46] Because our results suggested that *A odontolyticus* is involved in the initiation of CRC consistent with the results that *A odontolyticus* is abundantly present in the feces of early CRC patients,[11] preventive methods against colonic tumorigenesis need to be developed on the basis of the findings. Because bacterial MVs can penetrate the mucosal barrier and interact with the internal cells,[47] nanotechnology with accurate species-specific mechanisms such as nanoparticles or phage therapy as well as antimicrobial therapy may be better in delivering effects against *A odontolyticus* or its MVs.

In conclusion, *A odontolyticus*, abundant in the feces of patients with early CRC, secretes MVs, which induce excessive ROS production in colon epithelial cells, leading to colonic dysplasia.

Methods

Cells

SV40-immortalized human colon epithelial cells (iCECs) were purchased from ABM Company (#T0570, Richmond, BC, Canada) and cultured in Dulbecco modified Eagle medium (DMEM) supplemented with 5% fetal bovine serum and 1% penicillin–streptomycin. HT29 and HCT116 were purchased from American Type Culture Collection (ATCC), and C57BL/6 mouse embryo fibroblasts (MEFs) were purchased from Oriental Bio Service (Kyoto, Japan). HT29, HCT116, and MEFs were cultured in DMEM supplemented with 10% fetal bovine serum and 1% penicillin–streptomycin.

Bacterial Cultures

A odontolyticus (ATCC 17929) and *F nucleatum* (ATCC 25586) were provided by Prof. Imai K (Department of Microbiology and Immunology, Nihon University School of Dentistry, Tokyo, Japan). Both bacteria were cultured in Gifu anaerobic medium (Nissui Pharmaceutical Co, Tokyo, Japan) at 37°C. *A odontolyticus* was maintained under aerobic conditions, and *F nucleatum* was maintained under anaerobic conditions in an anaerobic jar with an Anaero-Pack (Mitsubishi Gas Chemical Company, Inc, Tokyo, Japan). *E coli* strain DH5α (Nippon Gene, Tokyo, Japan) was cultured in Luria–Bertani (Difco; BD Biosciences, Franklin Lakes, NJ) medium aerobically at 37°C. *Lacticaseibacillus rhamnosus* (NCTC 12953, recently reclassified from *Lactobacillus*[48]) was purchased from the National Collection of Type Cultures and cultured in Man–Rogosa–Sharpe medium (#556-36925, Fujifilm Wako Pure Chemical, Osaka, Japan) at 37°C in anaerobic conditions.

Reagents

BAY 11-7082 (#020-17871, Fujifilm Wako Pure Chemical) was used at 2 μmol/L. JSH-23 (#HY-13982, MedChem Express, NJ) was used at 10 μmol/L. LTA and peptidoglycan

Figure 7. (***See previous page***). **Increased ROS production by A.o MVs is dependent on its internalization by DNM-mediated endocytosis.** (*A*) Relative ROS levels of WT or TLR2^{ko} in iCECs at 24 hours after A.o MVs (20 μg/mL) treatment. Data are shown as mean ± SD of 3 biological replicates (n = 3). *P* values were calculated using one-way ANOVA followed by Tukey's test. (*B*) Relative ROS levels of iCECs at 24 hours after A.o MVs (20 μg/mL) treatment with or without NF-κB inhibitors (n = 3). Data are shown as mean ± SD of 3 biological replicates (n = 3). *P* values were calculated using one-way ANOVA followed by Tukey's test. (*C*) Labeled MVs and ECGreen (5 μmol/L), which stains only internalized endosomes, were added to iCECs and incubated at 37°C for 4 hours. Representative fluorescence images of internalized MVs. Although internalized A.o MVs were co-localized with endosomes at 37°C, MVs did not enter the cell and remained outside the cell at 4°C. *Red*, labeled MVs; *green*, endosomes; *blue*, nuclei stained with Hoechst. Scale bars represent 20 μm. (*D*) Representative fluorescence images of internalized A.o MVs in WT or TLR2ko iCECs. *Red*, labeled MVs; *blue*, nuclei (stained with DAPI). Scale bars represent 20 μm. *Right*: quantification of the fluorescence levels. Data are shown as mean ± SD of 3 technical replicates (n = 3). *P* values were calculated using two-sided Welch's *t* test. (*E*) Cytotoxicity analysis for inhibitors of endosomes. After each inhibitor was incubated with iCECs for 24 hours, cell viability was measured using a cell counting assay. Data are shown as mean ± SD of 3 biological replicates (n = 3). (*F*) Representative images of A.o MVs internalization under the treatment of endocytosis inhibitors. *Red*, labeled MVs; *blue*, nuclei stained with DAPI. Scale bars represent 20 μm. *Right*: quantification of the fluorescence levels. Data are shown as mean ± SD of 3 technical replicates (n = 3). *P* values were calculated using one-way ANOVA followed by Tukey's test. (*G*) Relative ROS levels in iCECs at 24 hours after A.o MVs treatment with or without endocytosis inhibitors. Data are shown as mean ± SD of 3 biological replicates (n = 3). *P* values were calculated using one-way ANOVA followed by Tukey's test. (*H*) *Left*, mRNA levels of *DNM1, DNM2*, and *DNM3* normalized to *ACTB* in iCECs shown in biological triplicates. Differences in CT (cycle threshold) values between each gene and *ACTB* defined as ΔCT. Data are shown as mean ± SD of 3 biological replicates (n = 3). *Right*, confirmation of DNM1 and DNM2 knockdown in iCECs by Western blotting. (*I*) Relative ROS levels in iCECs with *DNM1* or *DNM2* knocked down by siRNA, 24 hours after treatment with PBS or A.o MVs (20 μg/mL). Data are shown as mean ± SD of 3 biological replicates (n = 3). *P* values calculated using one-way ANOVA followed by Tukey's test. (*J*) Cytotoxicity analysis for inhibitors of endosomal acidification. After each inhibitor was incubated with iCECs for 24 hours, cell viability was measured using a cell counting assay. Data are shown as mean ± SD of 3 biological replicates (n = 3). (*K*) Relative ROS levels in iCECs 24 hours after A.o MVs are treated with or without inhibitors of endosomal maturation and acidification. Data are shown as mean ± SD of 3 biological replicates (n = 3). *P* values were calculated using one-way ANOVA followed by Tukey's test.

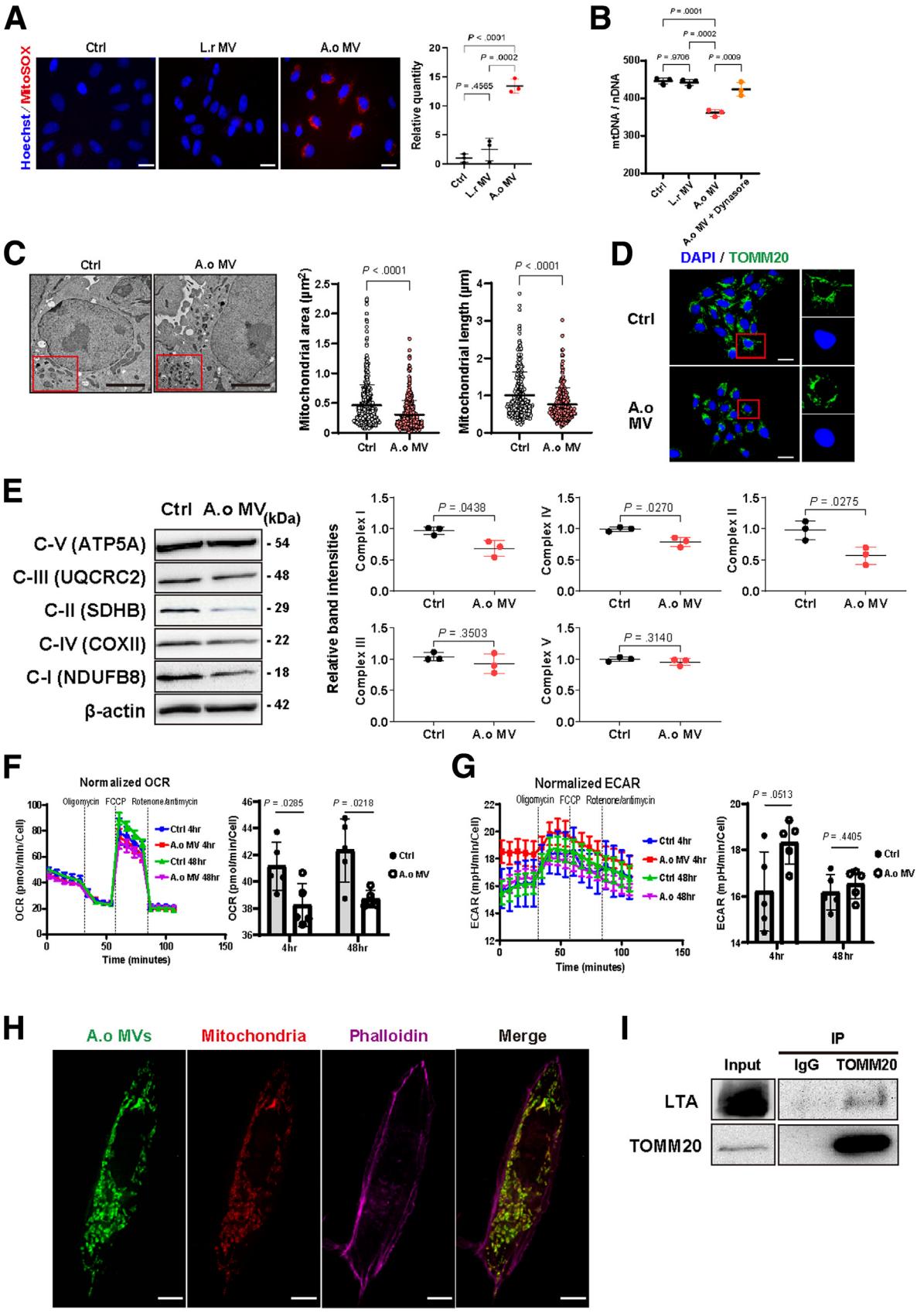
A
Ctrl
L.r MV
A.o MV
Hoechst / MitoSOX
Relative quantity
P < .0001
P = .0002
P = .4565
B
mtDNA / nDNA
P = .0001
P = .0002
P = .9706
P = .0009
Ctrl
L.r MV
A.o MV
A.o MV + Dynasore
C
Ctrl
A.o MV
Mitochondrial area (μm²)
Mitochondrial length (μm)
P < .0001
D
DAPI / TOMM20
Ctrl
A.o MV
E
Ctrl A.o MV (kDa)
C-V (ATP5A)
C-III (UQCRC2)
C-II (SDHB)
C-IV (COXII)
C-I (NDUFB8)
β-actin
54
48
29
22
18
42
Relative band intensities
Complex I
Complex IV
Complex II
Complex III
Complex V
P = .0438
P = .0270
P = .0275
P = .3503
P = .3140
F
Normalized OCR
Oligomycin
FCCP
Rotenone/antimycin
Ctrl 4hr
A.o MV 4hr
Ctrl 48hr
A.o MV 48hr
OCR (pmol/min/Cell)
Time (minutes)
P = .0285
P = .0218
4hr
48hr
G
Normalized ECAR
ECAR (mpH/min/Cell)
P = .0513
P = .4405
H
A.o MVs
Mitochondria
Phalloidin
Merge
I
IP
Input
IgG
TOMM20
LTA
TOMM20

from *Staphylococcus aureus* were purchased from Sigma-Aldrich (#77140, St Louis, MO). N-acetyl-L-cysteine (#017-05131, Fujifilm Wako Pure Chemical) was used at 5 μmol/L. The chemical inhibitors of endocytosis used were as follows: Dynasore (20 μmol/L, #D5461, Tokyo Chemical Industry, Tokyo, Japan) and Dyngo 4a (30 μmol/L, #S7163, Selleck Chemicals, Houston, TX) to inhibit dynamin-dependent endocytosis,[49,50] Filipin III (5 μmol/L, #70440, Fujifilm Wako Pure Chemical) to inhibit lipid rafts/caveolae-mediated endocytosis,[51] Chlorpromazine (2 μmol/L, #C2481, Tokyo Chemical Industry) to clathrin-mediated endocytosis,[52] Cytochalasin D (1 μmol/L, #140-08531, Fujifilm Wako Pure Chemical) to inhibit micropinocytosis,[53] and Nocodazole (0.5 μmol/L, #140-08531, Fujifilm Wako Pure Chemical) to inhibit polymerization of microtubule cytoskeleton.[54] The reagents used to inhibit endosomal maturation and acidification included bafilomycin A1 (0.5 μmol/L, #11038, Fujifilm Wako Pure Chemical), which inhibits endosomal acidification by blocking endosomal ATPase,[55] monensin sodium salt (1 μmol/L, #M2573, Tokyo Chemical Industry), which disrupts the proton gradient across vesicular membranes to prevent endosome acidification,[56] and chloroquine diphosphate (10 μmol/L, #038-17971, Fujifilm Wako Pure Chemical), which increases the pH inside endocytic vesicles to inhibit endosome acidification.[57] The optimal concentration of these inhibitors was determined through cytotoxicity assays.

Western Blotting

Cells were lysed in lysis buffer (50 mmol/L Tris-HCl [pH 7.4], 150 mmol/L NaCl, 1% NP40, and 0.1% sodium dodecyl sulfate [SDS]) for 15 minutes on ice, and cellular debris was cleared by centrifugation at 15,000 rpm for 10 minutes. The lysates were added to 4× sample buffer, and the mixture was boiled at 95°C for 5 minutes. MVs or proteins extracted by bacteria were lysed in 4× sample buffer, and the mixture was boiled at 95°C for 5 minutes. The samples were separated on a 10%–20% gradient polyacrylamide gel (Fujifilm Wako Pure Chemical) by SDS-polyacrylamide gel electrophoresis, followed by electrical transfer to polyvinylidene difluoride membranes (Merck Millipore, Burlington, MA). The Precision Plus Protein All Blue Protein Standards (Bio-Rad, Hercules, CA) were used to estimate molecular weights. After blocking with 5% dry milk, the membranes were probed with the appropriate primary antibodies diluted in Immunoshot Reagent 1 (Cosmo Bio Co., Ltd, Tokyo, Japan) overnight at 4°C. The corresponding horseradish peroxidase-conjugated secondary antibodies (GE Healthcare, Little Chalfont, UK) were subsequently applied. Bound antibodies were detected using Immunostar LD Reagents (Fujifilm Wako Pure Chemical), and images were acquired using a WSE-6100 LuminoGraph I instrument (Atto, Tokyo, Japan). Band intensities were analyzed using ImageJ software (National Institutes of Health, Bethesda, MD). The primary antibodies are listed in Table 1.

Immunofluorometric Assay

Cells were fixed with 4% paraformaldehyde in 1× PBS for 15 minutes at room temperature and permeabilized with 0.1% Triton-X in 1× PBS for 20 minutes at room temperature. After 3 washes, cells were incubated with 5% normal goat serum for 30 minutes for blocking. Next, primary antibodies diluted in Can Get Signal Immunostaining Solution B (Toyobo, Osaka, Japan) were used, and the samples were incubated overnight at 4°C. Cells were incubated with the corresponding secondary antibodies conjugated to Alexa 488 or 555 (Molecular Probes, Eugene, OR, 1:300 or 500) diluted in Can Get Signal Immunostaining Solution B for 30 minutes at room temperature in the dark. After additional washes, the slides were mounted with a fluorescence mounting medium containing 4′,6-diamidino-2-phenylindole (DAPI; #H-1200; Vector Laboratories, Burlingame, CA). In some cases, the slides were incubated with Hoechst 33342 (Fujifilm Wako Pure Chemical) for 10 minutes and covered with fluorescence mounting medium (#S3023, DAKO, Carpinteria, CA) and

Figure 8. (*See previous page*). Internalized A.o MVs are co-localized with mitochondria, leading to its dysfunction by impairing OXPHOS. (*A*) Representative fluorescence images of mitochondrial superoxide using Mito-Sox in iCECs at 24 hours after MV treatments. Scale bars represent 20 μm. *Right*: quantification of the fluorescence levels. Data are shown as mean ± SD of 3 technical replicates (n = 3). *P* values were calculated using one-way ANOVA followed by Tukey's test. (*B*) Mitochondrial DNA (mtDNA) levels normalized to nuclear DNA (nDNA) levels in 100 ng of total DNA from iCECs at 24 hours after MV treatment (n = 3). Data are shown as mean ± SD. *P* values were calculated using one-way ANOVA followed by Tukey's test. (*C*) Representative transmission electron microscopy (TEM) images of mitochondria in iCECs treated with PBS or A.o MVs for 48 hours. Analyses of the area (μm^2) and length (μm) of mitochondria (n > 200) are shown in *right panels*. Data are shown as mean ± SD. *P* values were calculated using the 2-sided Mann–Whitney U test. (*D*) Representative immunofluorescence images of TOMM20 in iCECs at 24 hours after A.o MVs treatment (20 μg/mL) or PBS. Scale bars represent 20 μm. (*E*) Western blotting results of OXPHOS complex subunits (C-I, II, III, IV, and V) at 48 hours after treatment with PBS or A.o MVs. Relative band intensities normalized to β-actin are shown in *right panels*. Data are shown as mean ± SD of 3 technical replicates (n = 3). (*F*) Real-time OCR was measured during sequential treatments with oligomycin (ATP-synthase inhibitor), FCCP (uncoupler), and rotenone/antimycin (ETC inhibitors), as shown in *left panel*. Basal OCR results are shown in *right panel*. Data are shown as mean ± SD of 5 biological replicates (n = 5). *P* values were calculated using two-way ANOVA test. (*G*) Real-time extracellular acidification rate (ECAR) was measured during sequential treatments with oligomycin, FCCP, and rotenone/antimycin (*left panel*). Basal ECAR was also analyzed (*right panel*). Data are shown as mean ± SD of 5 biological replicates (n = 5). *P* values were calculated using two-way ANOVA test. (*H*) Representative confocal fluorescence images demonstrating the co-localization of A.o MVs (*green*) and mitochondria (*red*); cytoskeleton is labeled with phalloidin (*purple*). Scale bars represent 5 μm. (*I*) A.o MVs and intact mitochondria mixture subjected to co-immunoprecipitation (IP) using an anti-TOMM20 antibody, with an anti-isotype antibody (normal mouse immunoglobulin G) as negative control. Precipitated proteins analyzed by Western blotting using antibodies against TOMM20 and LTA. A portion of the mixture was used as the input for the analysis.

observed using DMi8 (Leica, Wetzlar, Germany). The antibodies used are listed in Table 1.

Paraffin-embedded intestinal sections of human iPSC-derived intestinal organoids and BALB/c mouse colon tissues were used for immunofluorescence analyses. The sections were deparaffinized with Histo-Clear (National Diagnostics, GA) and ethanol, followed by antigen retrieval with an autoclave at 121°C for 10 minutes. After incubation with the blocking buffer (10% goat serum in PBS) at room temperature for 30 minutes, sections were stained with the primary antibodies diluted in Can Get Signal Immunostain Solution B at 4°C overnight. After three 5-minute washes in PBS, tissues sections were reacted for 1 hour at room temperature with corresponding secondary antibodies diluted in Can Get Signal Immunostain Solution B. After additional washes, coverslips were applied using a DAPI-containing embedding medium (#H-1200; Vector Laboratories). Images were acquired using a DMi8 fluorescence microscope. The primary antibodies used are listed in Table 1. The fluorescence intensity of the images was quantified using ImageJ software.

Immunohistochemistry

Paraffin-embedded intestinal organoids and mouse colon tissues were used. After deparaffinization and antigen retrieval, endogenous peroxidase activity was blocked by 3% hydrogen peroxide for 10 minutes. After blocking for 30 minutes, the sections were incubated overnight at 4°C with primary antibody, followed by incubation with horseradish peroxidase-conjugated secondary antibodies (Nichirei Bioscience, Tokyo, Japan) for 30 minutes. Probes were visualized using 3,3′-diaminobenzidine in the buffered substrate (Nichirei Bioscience). Images were acquired using the Olympus DP72 microscope digital camera system. The primary antibodies used are listed in Table 1.

RNA Isolation, Reverse Transcription, and Quantitative Polymerase Chain Reaction

Total RNA was isolated using an ISOGEN II (Nippon Gene) according to the manufacturer's protocol. Complementary DNA was synthesized using the ReverTra Ace qPCR RT Master Mix with gDNA Remover (Toyobo). To determine IL-6, IL-8, and TNFα levels, quantitative reverse transcription-polymerase chain reaction was performed using SYBR qPCR Mix (Toyobo) with the StepOnePlus Real-Time PCR System (Life Technologies, Carlsbad, CA). The average threshold cycle number (Ct) values were normalized to those of actin and calculated using the delta-delta Ct (ddCt) method. The primer sequences used are listed in Table 2.

Cell Attachment Assay

The assays were performed as previously described.[17] Briefly, cells were seeded in 24-well plates at 8.0×10^4 cells per well in the growth medium and grown until 100% confluency. Bacteria were added to the cells at a multiplicity of infection of 50. After incubation at 37°C in 5% CO_2 for 1 hour, the cells were washed 3 times with PBS (pH 7.1) supplemented with $Ca^{2+}$and Mg^{2+}. Next, the cells were lysed with water for 20 minutes at 37°C. The lysates serially

Table 1. Antibodies Used in This Study

Antibodies	Application, dilution	Catalog no.	Supplier
IκBα	WB, 1:20,000	ab32518	Abcam
Phospho-IκBα	WB, 1:1000	9246	Cell Signaling Technology
β-actin	WB, 1:10,000	5125	Cell Signaling Technology
NF-κB p65	IFC, 1:800	6956	Cell Signaling Technology
Toll-like receptor 2	WB, 1:1000	12276	Cell Signaling Technology
MYD88	WB, 1:1000	4283	Cell Signaling Technology
Lipoteichoic acid	WB, 1:1000; IFC, 1:100	HM2048	Hycult Biotech
Peptidoglycan	WB, 1:1000	GTX39437	GENETEX
Phospho-Histone H2A.X (γH2AX)	WB, 1:1000; IFC, 1:800; IF, 1:800; IHC, 1:480	9718	Cell Signaling Technology
P21 Waf1/Cip1	WB, 1:1000	2947	Cell Signaling Technology
Villin	IHC, 1:100	ab130751	Abcam
Lysozyme	IHC, 1:50	ab108508	Abcam
Chromogranin A (Chr-A)	IHC, 1:50	sc-393941	Santa Cruz Biotechnology
CDX2	IF, 1:250	ab76541	Abcam
Alpha-smooth muscle actin (α-SMA)	IF, 1:200	ab7817	Abcam
Cadherin-17	IF, 1:100	MAB1032	R&D Systems
MUC2	IF, 1:180	ab90007	Abcam
Dynamin (DNM) I	WB, 1:200	sc-58260	Santa Cruz Biotechnology
Dynamin (DNM) II	WB, 1:100	sc-166669	Santa Cruz Biotechnology
TOMM20	IP, 1:200; WB, 1:1000	ab56783	Abcam
Normal mouse IgG	IP, 1:200	140-09511	Fujifilm Wako Pure Chemical

diluted were plated onto agar plates. After 2 days of incubation at 37°C, bacterial colonies in the plates were counted. The attachment levels were determined as the percentage of bacteria recovered after cell lysis compared with the total number of bacteria initially added.

Transwell Co-culture Assay

Cells were seeded in the bottom chamber of 6.5-mm Transwell inserts (#3470, Corning, Tewksbury, MA) at 8.0×10^4 cells, and bacteria were seeded in the top chamber at a multiplicity of infection of 50 for the indicated time.

MV Isolation and Examination of the Quantity and Size Distribution

MVs were isolated on the basis of previous reports.[58,59] Bacteria were cultured in broth until 1.8 at OD 600 nm measured by CO 8000 Biowave Personal Cell Density Meter (WPA, Biochrom Ltd, Cambridge, UK). After twice centrifugation of bacterial cultures at 10,000*g* for 10 minutes, the supernatants were filtered through 0.45 and 0.22 μm polyvinylidene difluoride filters. The filtered supernatants were concentrated and removed small molecules using an Amicon Ultra-15 100K (Merck Millipore). The MVs were pelleted from the concentrated supernatants by ultracentrifugation at 100,000*g* for 2 hours at 4°C. The MVs were then resuspended in 150 μL PBS to prepare crude MVs. For qEV size exclusion chromatography, qEV columns (single 35) with an automated fraction collector (Izon Science, Christchurch, New Zealand) were used according to the manufacturer's instructions. Briefly, the column was flushed with 10 mL PBS before use. Then, 150 μL of crude MVs was loaded into the top filter of the column. The automated fraction collector was programmed to discard the first 1 mL, and 0.6 mL fraction was collected. The protein concentration of isolated MVs was determined by the Qubit Protein Assay kit and Qubit 4 Fluorometer (Thermo Fisher Scientific, Waltham, MA).

The quantity and size distribution of isolated MVs were determined using nanoparticle tracking analysis by NanoSight LM10 (Malvern Instruments Ltd, UK) as previously described.[60] Briefly, MVs were diluted in PBS (-) at a final concentration of 10^8–10^9 particles per mL according to the manufacturer's guidelines. Capture settings were as follows: camera gain of 13, camera level of 10, and detection threshold of 5. Reads of 60-second duration were performed 5 times per sample at 25°C. Analyses were performed according to the manufacturer's protocol.

Table 2. Primers Used in This Study

Gene	Sequence (5′→3′)
Human IL-8	Fw: CTTGTCATTGCCAGCTGTGT Rv: TGACTGTGGAGTTTTGGCTG
Human TNFα	Fw: CAGAGGGAAGAGTTCCCCAG Rv: CCTTGGTCTGGTAGGAGACG
Human β-actin	Fw: CTGTGCTACGTCGCCCTGG Rv: GCCACAGGACTCCATGCCC
Human dynamin-1	Fw: GCTGACTGCTGAGAATCTGTCC Rv: GTGTCTCACAGGCTAGCTCCAG
Human dynamin-2	Fw: CATGATCCTGCAGTTCATCAGC Rv: CTTCTCAACGGGAGCAACTTGT
Human dynamin-3	Fw: ACTCCAGCCAACACTGATCTTGC Rv: CCCCTGCGAAGAGGCAACAGT
Mouse IL-6	Fw: TAGTCCTTCCTACCCCAATTTCC Rv: TTGGTCCTTAGCCACTCCTTC
Mouse TNFα	Fw: AAGCCTGTAGCC CACGTCGTA Rv: GGCACCACTAGTTGGTTGTCTTTG
Mouse β-actin	Fw: AGTGTGACGTTGACATCCGT Rv: GCAGCTCAGTAACAGTCCGC

Luciferase Assay

Cells cultured in the 6-cm dish were transfected with 0.2 μg of pGL4.74[hRluc/TK] and 2 μg of NF-κB luc used FuGene 6 Transfection Reagent (Roche, Basel, Switzerland). After 24 hours, the transfected cells were split into 12-well plates at 4.0×10^4 cells per well. The next day, stimulators were added for the indicated time, and the cells were harvested. The cellular lysates were analyzed for luciferase activity using Dual-Luciferase Reporter Assay System (Promega, Madison, WI). The firefly luciferase activity values were corrected using the values obtained from the Renilla luciferase activity as a control.

Gene Knockout

CRISPR-mediated gene knockout in iCECs was carried out as follows: designed guide RNAs were cloned into LentiCRISPRv2 neo (#98292, Addgene, Cambridge, MA). To produce and package infectious lentivirus, HEK293T cells (ATCC) were co-transfected with LentiCRISPRv2-sgRNA and lentiviral plasmid packaging mix (pPACK Lentivector Packaging Kit, System Bioscience, Palo Alto, CA) using the Effectene Transfection Reagent (Qiagen, Gelderland, Netherlands). After 48 hours, the supernatant was collected and passed through a 0.45-μm filter. Viruses were concentrated using the PEG-it virus precipitation solution (System Biosciences, Mountain View, CA). After precipitating for 24 hours, the viruses were collected and diluted with PBS (–) Cells seeded in 6-well plates were transduced with the diluted viruses using polybrene (10 μg/mL, Santa Cruz Biotechnology, Dallas, TX). After 48 hours, cells were subjected to G-418 sulfate (#074-06801, Fujifilm Wako Pure Chemical) for 7 days. Western blotting was done to confirm the efficient knockout of the target gene.

siRNA-mediated Gene Silencing

For siRNA-mediated knockdown, cells were transfected with siRNAs at the following concentrations: 10 μmol/L DNM1 siRNA (Dharmacon, ON-TARGETplus SMARTpool siRNA, catalog no. L-003940-00-0005) or 10 μmol/L DNM2 siRNA (Dharmacon, ON-TARGETplus SMARTpool siRNA, catalog no. L-004007-00-0005). For the control sample, cells were transfected with 10 μmol/L non-targeting pool siRNA (Dharmacon, ON-TARGETplus, catalog no. D-001810-10-05). The transfection was performed using Lipofectamin

RNAiMAX Transfection Reagent (#13778075, Invitrogen, CA), according to the manufacturer's protocol.

Extraction of the Lysate and the Membrane Protein of A odontolyticus

A odontolyticus lysate was extracted according to the methods described previously.[61] Briefly, *A odontolyticus* were grown overnight at 37°C in 200 mL of GAM broth; the bacteria were collected by centrifugation at 16,000*g* for 10 minutes and washed twice with PBS. After centrifugation, cell pellets were resuspended in TE buffer and sonicated 30 seconds × 10, 30-second intervals. Then the solution was centrifuged at 16,000*g* × 0 min. The supernatant was collected and measured concentrations using a Protein Assay kit and Qubit 4 Fluorometer and stored at –20°C until use.

The membrane proteins of *A odontolyticus* were extracted according to the methods described previously.[62] *A odontolyticus* were grown overnight at 37°C in 200 mL of GAM broth; the bacteria were collected by centrifugation at 16,000*g* for 10 minutes and washed twice with PBS. After centrifugation, cell pellets were resuspended in 40 mL of osmotic digestion buffer containing 20% sucrose in 20 mmol/L Tris–HCl, pH 7.0, 10 mmol/L $MgCl_2$, protease inhibitor cocktail (Sigma-Aldrich) and 10 U of mutanolysin (Sigma-Aldrich), followed by shaking 2 hours at 37°C. Then, the solution was centrifuged at 3000*g* for 1 hour to remove protoplasts, followed by centrifugation at 16,000*g* for 30 minutes to remove cell debris. The supernatant was collected and measured concentrations using the Protein Assay kit and Qubit 4 Fluorometer.

LTA Inactivation

LTA inactivation was performed with platelet-activating factor–acetylhydrolase[63] or NaOH.[64] For diacylation by platelet-activating factor–acetylhydrolase, A.o MVs were incubated with 30 μg/mL of platelet-activating factor–acetylhydrolase (#2544185, Fujifilm Wako Pure Chemical) at 37°C for 12 hours. After incubation the reaction mixture was inactivated by adding 100 μmol/L Pefabloc SC (#76307, Sigma-Aldrich). For degradation by NaOH hydrolysis treatment, 9 volumes of A.o MVs were added to 1 volume of 2 N NaOH and incubated at 37°C for 2 hours. After incubation, the mixture was neutralized with 6 N HCl to obtain a pH of 6.5–7.5.

Examination of the Internalization of MVs

To visualize MVs fluorescently, A.o MVs were labeled using the ExoSparkler Exosome Membrane Labeling Kit-Red (Dojindo, Kumamoto, Japan), which can label lipid bilayers, according to the manufacturer's instructions. To examine the endocytosis, cells were cultured on μ-slide (#ib80421, ibidi GmbH, Munich, Germany) for 24 hours. Labeled MVs and ECGreen-Endocytosis Detection Dye (Dojindo), which is not membrane permeable and internalized by endocytosis, were added and incubated at 37°C for 4 hours. After 3 washings, DMEM was added in the chambers and observed living cells using a DMi8 fluorescence microscope. For assessment of the inhibition of endocytosis, cells were cultured on 4-well chamber slides for 24 hours. After endocytosis inhibitors were preincubated for 1 hour, labeled MVs were added and incubated for 4 hours. After washing 3 times, cells were fixed with 4% paraformaldehyde in 1× PBS for 15 minutes at room temperature, and the slides were mounted with fluorescence mounting medium containing DAPI. The fluorescence observation was performed using DMi8.

Transmission Electron Microscopy

To visualize MVs, transmission electron microscopy was performed. MVs were fixed in phosphate-buffered 2% glutaraldehyde and stained with uranyl acetate. MVs were then examined using a JOEL JEM 2000EX transmission electron microscope (Hanaichi Ultrastructure Research Institute, Japan).

Transmission electron microscopy ultrathin sections were used to visualize MVs at the bacterial surface or the morphology of the mitochondria. Bacterial pellets or iCECs cultured to 100% confluently in 6-well plates were fixed in phosphate-buffered 2% glutaraldehyde and subsequently post-fixed in 2% osmium tetraoxide for 2 hours in the ice bath. Then, the specimens were dehydrated in graded ethanol and embedded in epoxy resin. Ultrathin sections were obtained by ultramicrotome technique and were stained with uranyl acetate for 15 minutes and with a staining solution for 2 minutes. Stained samples were subjected to transmission electron microscopy observation at 100 kV (JEM-1400Flash, JEOL). Mitochondrial length and area were analyzed using ImageJ software (National Institutes of Health).

Proteomic Analyses of MVs by Liquid Chromatography–Mass Spectrometry

After 2 μg of MVs was separated by SDS–polyacrylamide gel electrophoresis, the gel was stained using a silver staining kit (Integrale, Tokushima, Japan). Selected bands were cut out, and the corresponding peptides were identified using liquid chromatography–mass spectrometry (Integrale). All mass spectrometry data were analyzed using Mascot (Matrix Science, London, UK; version 2.8.0.1). The mascot was set up to search the UniProtKB_Schaalia odontolytica_220207 database (13,736 entries) assuming the digestion enzyme trypsin. Mascot was searched with a fragment ion mass tolerance of 0.020 Da and a parent ion tolerance of 5.0 PPM. Oxidation of methionine and propionamide of cysteine was specified in Mascot as variable modifications. Scaffold (version Scaffold_5.1.2, Proteome Software Inc, Portland, OR) was used to validate the mass spectrometry–based identification of the peptides and proteins using the specific threshold for their accuracy. Proteins that contained similar peptides and could not be differentiated on the basis of the mass spectrometry analyses were grouped to satisfy the principles of parsimony. Proteins sharing significant peptide sequences were grouped into clusters.

Measurements of Cellular ROS Levels

Cellular ROS levels were measured using the ROS-Glo H2O2 Assay Kit (Promega). Briefly, 1.0×10^4 cells were cultured in 96-well white-walled plates with clear bottoms. After treating for 24 hours, 20 μL of the H_2O_2 substrate solution was added, followed by incubation for 2 hours. Then, 100 μL of ROS-Glo Detection Solution was added, the plate was incubated at room temperature for 20 minutes, and luminescence was measured using a GloMax 96 Microplate Luminometer (Promega).

Cell-Cycle Analyses

Cells cultured in a 6-well plate were treated with A.o MVs for 48 hours and then harvested. The cells were fixed in ice-cold 70% ethanol and incubated overnight at −20°C. The fixed cells were washed twice with PBS and resuspended in 990 μL of PBS. RNA contamination was excluded by adding 10 μL ribonuclease solution (Nippon Gene; 10 mg/mL) and incubating for 30 minutes at room temperature. Cellular DNA was stained by adding 50 μL of propidium iodide (1 μg/μL in PBS, Fujifilm Wako Pure Chemical) and incubated for 1 minute at room temperature in the dark. Flow cytometry analyses were done using the Guava Easy Cyte Plus instrument (GE Healthcare).

Colony Formation Assay

iCECs were seeded in a 12-well plate, treated with 20 μg/mL of A.o MVs or PBS every 3 days, and passaged every 7 days. After 3 months, a colony formation assay using the soft agar was performed as follows. First, 6-well plates were bottom-layered with 2 mL of 0.6% agarose and 10% fetal bovine serum and 1% penicillin-streptomycin supplemented DMEM. After the bottom layer solidified, the top layer containing 1.0×10^4 cells/plate, 0.35% agarose, and 10% fetal bovine serum–supplemented DMEM was added. The plates were incubated at 37°C for another 2 weeks. Finally, colonies were stained with 0.005% crystal violet. The images of the plates were analyzed using ImageJ software.

Cytotoxicity by Endocytosis Inhibitors

Cell Counting Kit-8 (Dojindo) was used for the cytotoxicity test. The 1.0×10^4 cells were seeded onto 96-well plates and incubated at 37°C. On the next day, cells were treated with inhibitors or dimethyl sulfoxide as a control. After 24 hours, 10 μL of CCK-8 solution was added to each well, and the cells were incubated for 3 hours. Absorbance at 450 nm was measured to calculate the cell viability using a microplate reader (Thermo Fisher Scientific). The absorbance values were standardized against those from the blank well.

Organoid Model

The human induced pluripotent stem cell-derived apical-out gut organoids, purchased from Dai Nippon Printing (Tokyo, Japan), were cultured without Matrigel or extracellular matrix, as reported previously.[65] The organoids were cultured in xenogeneic-free medium containing 85% Knockout DMEM (Life Technologies, Carlsbad, CA) and 15% CTS Knockout SR XenoFree Medium (Life Technologies) supplemented with 2 mmol/L GlutaMAX supplement (Life Technologies), 0.1 mmol/L MEM Non-Essential Amino Acids solution (Life Technologies), 1% penicillin-streptomycin (Sigma-Aldrich), 50 μg/mL L-ascorbic acid (Fujifilm Wako Pure Chemical), 10 ng/mL heregulin-β-1 (Fujifilm Wako Pure Chemical), 200 ng/mL recombinant human IGF-1 (Fujifilm Wako Pure Chemical), and 10 ng/mL FGF2 (Fujifilm Wako Pure Chemical). The organoids were cultured with 20 μg of A.o MVs for 7 days. After treatment, the organoids were fixed at 4% paraformaldehyde for 3 hours at room temperature. Preparation of paraffin-embedded tissue sections, H&E staining, and alcian blue staining was performed by Septsapie (Tokyo, Japan).

Animal Studies

Following the current protocol, which allows for the use of sex- and age-matched mice,[66,67] we used 8-week-old female BALB/c mice (CLEA Japan, Tokyo, Japan). To each mouse, 20 μg A.o MVs diluted in 100 μL PBS were injected transanally weekly for 2 months. Control mice were injected with the same volume of PBS. The mice were euthanized at 3 days after the final injection. For the preparation of H&E stained or paraffin-embedded tissue sections, tissues were fixed in 10% formalin.

Mitochondrial Superoxide Levels

Mitochondrial superoxide levels were determined using MitoSOX Red (#M36008, Invitrogen). Briefly, 5.0×10^3 cells were cultured on μ-slide for 24 hours. After MVs treatment for 6 hours, cells were washed with PBS and incubated with 5 μmol/L of MitoSOX Red reagent in phenol red-free medium for 10 minutes, according to the manufacturer's protocol. The living cells were then gently washed 3 times with warm buffer and counterstained with Hoechst 33342. The fluorescent intensities were observed using the DMi8.

Quantification of Mitochondrial DNA Copy Number

The total DNA was isolated from 1.0×10^6 cells using the QIAamp DNA Mini Kit (QIAGEN) according to the manufacturer's protocol. Using the SYBR qPCR Mix (Toyobo), 100 ng of total DNA was subjected to quantitative polymerase chain reaction. The average Ct values of mitochondrial and nuclear DNAs were obtained. The relative levels of mitochondrial DNA were normalized to the levels of nuclear DNA. Human Mitochondrial DNA Monitoring Primer Sets (TaKaRa Bio, Shiga, Japan) targeting ND1 and ND5 as mitochondrial DNA and SLCO2B1 and SERPINA1 as nuclear DNA were used for the quantitation.

Detection of MVs and Mitochondrial Co-localization

To investigate the co-localization of MVs and mitochondria, MVs labeled with the ExoSparkler Exosome Membrane

Labeling Kit-Green (Dojindo) were added to iCECs seeded on 4-well chamber slides. The cells were incubated at 37°C for 4 hours. After 3 PBS washes, the cells were incubated with 500 nmol/L MitoTracke Red CMXRos at 37°C for 15 minutes and washed 3 times with PBS. The cells were fixed with 4% paraformaldehyde for 15 minutes at room temperature and permeabilized with 0.1% Triton-X in 1× PBS for 20 minutes at room temperature. Subsequently, the cytoskeleton was fluorescently labeled using the Phalloidin-iFluor 680 conjugate (AAT Bioquest, Sunnyvale, CA), following the manufacturer's protocol, and the nuclei were stained with DAPI. Images were captured using a spinSR10 confocal microscope imaging system (Evident, Japan).

Extraction of Intact Mitochondria

To extract intact mitochondria from cells, we established polyclonal iCECs stably expressing HA-MITO (HA-MITO iCECs) using pMXs-3XHA-EGFP-OMP25, as previously described.[68] After 1 wash with PBS, the cells were harvested in 1 mL of mitochondrial buffer (75 mmol/L sucrose, 225 mmol/L mannitol, 20 mmol/L HEPES, 0.5 mmol/L EDTA, pH 7). The cell suspension was centrifuged at 1000*g* for 2 minutes, the supernatant was discarded, and the cell pellet was resuspended in 500 μL of the same buffer. After cell homogenization, the homogenate was centrifuged at 1000*g* for 2 minutes, the supernatant was collected, and intact mitochondria were purified using the HA-tagged Protein Magnetic Purification Kit (#3342, Medical & Biological Laboratories, Tokyo, Japan) according to the manufacturer's protocol. All procedures were performed on ice.

Immunoprecipitation

Immunoprecipitation was performed to assess the binding of A.o MVs to the mitochondrial outer protein. This procedure used a TOMM20 antibody and Pierce Protein A/G Magnetic Beads (#88802, Thermo Fisher Scientific) according to the manufacturer's protocol. In brief, MVs were incubated with intact mitochondria extracted from HA-MITO iCECs, with rotation at room temperature for 3 hours. The mixture was incubated with the TOMM20 antibody or normal mouse immunoglobulin G (140-09511, Wako) as a negative control, with rotation overnight at 4°C. Subsequently, 50 μL of magnetic beads was added to the mixture and rotated for 30 minutes at 4°C. The beads were then separated using a magnetic separator and washed 3 times in buffer. Proteins bound to the beads were eluted using a low-pH solution and immediately neutralized. The eluates were mixed with 4× SDS sample buffer (0.25 mol/L Tris-HCl, 8% SDS, 40% glycerol, and 0.02% bromophenol blue, pH 6.8) and boiled at 95°C for 5 minutes. Western blotting was subsequently performed as previously described. To detect the proteins, TrueBlot anti-mouse immunoglobulin G horseradish peroxidase (diluted 1:1,000; Rockland Immunochemicals, Limerick, PA) was used as the secondary antibody to minimize interference from the heavy and light chains derived from the immunoprecipitated immunoglobulin.

RNA Sequencing

RNA sequencing was performed at the Rhelixa Co. (Tokyo, Japan). The total RNA of iCEC cells treated with or without 10 μg/mL of A.o MVs was isolated using ISOGEN II as described above and was treated by DNase. The purity of the total RNA samples was confirmed with an RNA integrity number >7, determined by a Bioanalyzer (Agilent), followed by the cDNA library preparation. Total RNA was converted to complementary DNAs with oligo dT primers using the NEBNext Poly (A) mRNA Magnetic Isolation Module (cat. no. E7490) and the NEBNext Ultra-TMII Directional RNA Library Prep Kit (cat. no. E7760). Complementary DNA libraries were sequenced with the NovaSeq 6000 system (Illumina) to produce 150 base pair-end reads.

Oxygen Consumption Rate and Extracellular Acidification Rate

OCR and extracellular acidification rate were measured using an extracellular flux analyzer (XFe 24; Agilent Technologies Inc, Santa Clara, CA), according to the manufacturer's protocols. Briefly, the Seahorse utility plate (Agilent Technologies Inc) containing calibrant media together with Seahorse injector port and probe plate was incubated overnight at 37°C without CO_2. On the day of the assay, the cell culture medium was replaced with a Seahorse XF assay buffer (supplemented with 10 mmol/L glucose, 1 mmol/L sodium pyruvate, and 2 mmol/L L-glutamine) and incubated in CO_2 free incubator at 37°C for at least half an hour. Then 8×10^4 cells were seeded in XF24 cell-culture microplates (#100777-004, Agilent Technologies Inc). OCR and extracellular acidification rate were measured after treatment with 20 μg/mL A.o MVs or PBS as a control for 4 or 48 hours. The designated injector ports were filled with the following MitoStress Test inhibitors: 0.5 μmol/L Oligomycin, 1 μmol/L Carbonyl cyanide-p-trifluoromethoxyphenylhydrazone (FCCP), and 0.25 μmol/L Rotenone and Antimycin. Oligomycin, FCCP, Rotenone, and Antimycin were purchased from Sigma-Aldrich.

Statistical Analyses

Statistical analyses were conducted using GraphPad Prism 9 (GraphPad Software, San Diego, CA). Continuous variables are reported as mean ± standard deviation (SD). Two-sample comparisons were performed using the 2-sided Welch *t*-test or two-way analysis of variance (ANOVA) test, and multiple comparisons were performed by the one-way ANOVA followed by Tukey test or Dunnett test. The 2-sided Mann–Whitney *U* test was used to compare data with a non-normal distribution. In all analyses, $P < .05$ was taken to indicate statistical significance.

References

1. Sung H, Ferlay J, Siegel RL, et al. Global Cancer Statistics 2020: GLOBOCAN estimates of incidence and mortality worldwide for 36 cancers in 185 countries. CA Cancer J Clin 2021;71:209–249.

2. Nistal E, Fernández-Fernández N, Vivas S, et al. Factors determining colorectal cancer: the role of the intestinal microbiota. Front Oncol 2015;5:220.
3. Brenner H, Kloor M, Pox CP. Colorectal cancer. Lancet 2014;383:1490–1502.
4. Díaz-Garrido N, Badia J, Baldomà L. Microbiota-derived extracellular vesicles in interkingdom communication in the gut. J Extracell Vesicles 2021;10:e12161.
5. Qin J, Li R, Raes J, et al. A human gut microbial gene catalogue established by metagenomic sequencing. Nature 2010;464:59–65.
6. Louis P, Hold GL, Flint HJ. The gut microbiota, bacterial metabolites and colorectal cancer. Nat Rev Microbiol 2014;12:661–672.
7. Kostic AD, Gevers D, Pedamallu CS, et al. Genomic analysis identifies association of Fusobacterium with colorectal carcinoma. Genome Res 2012;22:292–298.
8. Castellarin M, Warren RL, Freeman JD, et al. Fusobacterium nucleatum infection is prevalent in human colorectal carcinoma. Genome Res 2012;22:299–306.
9. Brennan CA, Garrett WS. Fusobacterium nucleatum: symbiont, opportunist and oncobacterium. Nat Rev Microbiol 2019;17:156–166.
10. Wong CC, Yu J. Gut microbiota in colorectal cancer development and therapy. Nat Rev Clin Oncol 2023, 10.1038:s41571-023-00766–x.
11. Yachida S, Mizutani S, Shiroma H, et al. Metagenomic and metabolomic analyses reveal distinct stage-specific phenotypes of the gut microbiota in colorectal cancer. Nat Med 2019;25:968–976.
12. Könönen E, Wade WG. Actinomyces and related organisms in human infections. Clin Microbiol Rev 2015;28:419–442.
13. Socransky SS, Haffajee AD. Dental biofilms: difficult therapeutic targets. Periodontol 2000 2002;28:12–55.
14. Yang Y, Weng W, Peng J, et al. Fusobacterium nucleatum increases proliferation of colorectal cancer cells and tumor development in mice by activating toll-like receptor 4 signaling to nuclear factor−κB, and up-regulating expression of microRNA-21. Gastroenterology 2017;152:851–866.e24.
15. Abed J, Emgård JEM, Zamir G, et al. Fap2 mediates Fusobacterium nucleatum colorectal adenocarcinoma enrichment by binding to tumor-expressed Gal-GalNAc. Cell Host Microbe 2016;20:215–225.
16. Gur C, Ibrahim Y, Isaacson B, et al. Binding of the Fap2 protein of Fusobacterium nucleatum to human inhibitory receptor TIGIT protects tumors from immune cell attack. Immunity 2015;42:344–355.
17. Rubinstein MR, Wang X, Liu W, et al. Fusobacterium nucleatum promotes colorectal carcinogenesis by modulating E-cadherin/β-catenin signaling via its FadA adhesin. Cell Host Microbe 2013;14:195–206.
18. Letourneau J, Levesque C, Berthiaume F, et al. In vitro assay of bacterial adhesion onto mammalian epithelial cells. J Vis Exp 2011:2783.
19. Deatherage BL, Cookson BT. Membrane vesicle release in bacteria, eukaryotes, and archaea: a conserved yet underappreciated aspect of microbial life. American Society for Microbiology Infection and Immunity 2012;80:1948–1957.
20. Brown L, Wolf JM, Prados-Rosales R, et al. Through the wall: extracellular vesicles in Gram-positive bacteria, mycobacteria and fungi. Nat Rev Microbiol 2015;13:620–630.
21. Bitto NJ, Cheng L, Johnston EL, et al. Staphylococcus aureus membrane vesicles contain immunostimulatory DNA, RNA and peptidoglycan that activate innate immune receptors and induce autophagy. J Extracell Vesicles 2021;10:e12080.
22. Champagne-Jorgensen K, Mian MF, McVey Neufeld KA, et al. Membrane vesicles of Lacticaseibacillus rhamnosus JB-1 contain immunomodulatory lipoteichoic acid and are endocytosed by intestinal epithelial cells. Sci Rep 2021;11:13756.
23. Kawai T, Akira S. Toll-like receptors and their crosstalk with other innate receptors in infection and immunity. Immunity 2011;34:637–650.
24. Akira S, Takeda K. Toll-like receptor signalling. Nat Rev Immunol 2004;4:499–511.
25. Tsoi H, Chu ESH, Zhang X, et al. Peptostreptococcus anaerobius induces intracellular cholesterol biosynthesis in colon cells to induce proliferation and causes dysplasia in mice. Gastroenterology 2017;152:1419–1433.e5.
26. Goodwin AC, Destefano Shields CE, Wu S, et al. Polyamine catabolism contributes to enterotoxigenic Bacteroides fragilis-induced colon tumorigenesis. Proc Natl Acad Sci U S A 2011;108:15354–15359.
27. Kang W, Jia Z, Tang D, et al. Fusobacterium nucleatum facilitates apoptosis, ROS generation, and inflammatory cytokine production by activating AKT/MAPK and NF-κB signaling pathways in human gingival fibroblasts. Oxid Med Cell Longev 2019;2019:1681972.
28. Singh M, Jadhav HR, Bhatt T. Dynamin functions and ligands: classical mechanisms behind. Mol Pharmacol 2017;91:123–134.
29. Yi A-K, Tuetken R, Redford T, et al. CpG motifs in bacterial DNA activate leukocytes through the pH-dependent generation of reactive oxygen species. J Immunol 1998;160:4755–4761.
30. Guo CY, Sun L, Chen XP, et al. Oxidative stress, mitochondrial damage and neurodegenerative diseases. Neural Regen Res 2013;8:2003–2014.
31. Nagdas S, Kashatus DF. The interplay between oncogenic signaling networks and mitochondrial dynamics. Antioxidants 2017;6:33.
32. Reznik E, Miller ML, Lu YS$_s$, et al. Mitochondrial DNA copy number variation across human cancers. Elife 2016;5:e10769.
33. Long X, Wong CC, Tong L, et al. Peptostreptococcus anaerobius promotes colorectal carcinogenesis and modulates tumour immunity. Nat Microbiol 2019;4:2319–2330.
34. Wu S, Rhee KJ, Albesiano E, et al. A human colonic commensal promotes colon tumorigenesis via activation of T helper type 17 T cell responses. Nat Med 2009;15:1016–1022.

35. DiDonato JA, Mercurio F, Karin M. NF-κB and the link between inflammation and cancer. Immunol Rev 2012; 246:379–400.
36. Taniguchi K, Karin M. NF-κB, inflammation, immunity and cancer: coming of age. Nat Rev Immunol 2018; 18:309–324.
37. Percy MG, Gründling A. Lipoteichoic acid synthesis and function in gram-positive bacteria. Annu Rev Microbiol 2014;68:81–100.
38. Bielaszewska M, Rüter C, Kunsmann L, et al. Enterohemorrhagic Escherichia coli hemolysin employs outer membrane vesicles to target mitochondria and cause endothelial and epithelial apoptosis. PLoS Pathog 2013; 9:e1003797.
39. Deo P, Chow SH, Hay ID, et al. Outer membrane vesicles from Neisseria gonorrhoeae target PorB to mitochondria and induce apoptosis. PLoS Pathog 2018;14:e1006945.
40. Kozjak-Pavlovic V, Ross K, Rudel T. Import of bacterial pathogenicity factors into mitochondria. Curr Opin Microbiol 2008;11:9–14.
41. Nougayrède JP, Donnenberg MS. Enteropathogenic Escherichia coli EspF is targeted to mitochondria and is required to initiate the mitochondrial death pathway. Cell Microbiol 2004;6:1097–1111.
42. Kenny B, Jepson M. Targeting of an enteropathogenic Escherichia coli (EPEC) effector protein to host mitochondria. Cell Microbiol 2000;2:579–590.
43. Ramachandran RP, Spiegel C, Keren Y, et al. Mitochondrial targeting of the enteropathogenic Escherichia coli map triggers calcium mobilization, ADAM10-MAP kinase signaling, and host cell apoptosis. mBio 2020; 11:e01397-20.
44. Caruana JC, Walper SA. Bacterial membrane vesicles as mediators of microbe–microbe and microbe–host community interactions. Front Microbiol 2020;11:432.
45. Bullman S, Pedamallu CS, Sicinska E, et al. Analysis of Fusobacterium persistence and antibiotic response in colorectal cancer. Science 2017;358:1443–1448.
46. Dong X, Pan P, Zheng D-W, et al. Bioinorganic hybrid bacteriophage for modulation of intestinal microbiota to remodel tumor-immune microenvironment against colorectal cancer. Sci Adv 2020;6:eaba1590.
47. Cecil JD, Sirisaengtaksin N, O'Brien-Simpson NM, et al. Outer membrane vesicle-host cell interactions. Microbiol Spectr 2019;7, 10.1128/microbiolspec.PSIB-0001–2018.
48. Zheng J, Wittouck S, Salvetti E, et al. A taxonomic note on the genus Lactobacillus: description of 23 novel genera, emended description of the genus Lactobacillus beijerinck 1901, and union of Lactobacillaceae and Leuconostocaceae. Int J Syst Evol Microbiol 2020; 70:2782–2858.
49. Macia E, Ehrlich M, Massol R, et al. Dynasore, a cell-permeable inhibitor of dynamin. Dev Cell 2006; 10:839–850.
50. Mccluskey A, Daniel JA, Hadzic G, et al. Building a better dynasore: the dyngo compounds potently inhibit dynamin and endocytosis. Traffic 2013;14:1272–1289.
51. Chew Y, Chung HY, Lin PY, et al. Outer membrane vesicle production by helicobacter pylori represents an approach for the delivery of virulence factors caga, vaca and urea into human gastric adenocarcinoma (Ags) cells. Int J Mol Sci 2021;22:3942.
52. Daniel JA, Chau N, Abdel-Hamid MK, et al. Phenothiazine-derived antipsychotic drugs inhibit dynamin and clathrin-mediated endocytosis. Traffic 2015;16:635–654.
53. Rennick JJ, Johnston APR, Parton RG. Key principles and methods for studying the endocytosis of biological and nanoparticle therapeutics. Nat Nanotechnol 2021; 16:266–276.
54. Goltz JS, Wolkofftt AW, Novikofft PM, et al. A role for microtubules in sorting endocytic vesicles in rat hepatocytes. Proc Natl Acad Sci U S A 1992; 89:7026–7030.
55. Marshansky V, Vinay P. Proton gradient formation in early endosomes from proximal tubules. Biochim Biophys Acta 1996;1284:171–180.
56. Maxfield FR. Weak bases and ionophores rapidly and reversibly raise the pH of endocytic vesicles in cultured mouse fibroblasts. J Cell Biol 1982;95:676–681.
57. Duve C De, Barsy T De, Poole B, et al. Commentary: lysosomotropic agents. Biochem Pharmacol 1974; 23:2495–2531.
58. Dauros Singorenko P, Chang V, Whitcombe A, et al. Isolation of membrane vesicles from prokaryotes: a technical and biological comparison reveals heterogeneity. J Extracell Vesicles 2017;6:1324731.
59. Athman JJ, Sande OJ, Groft SG, et al. Mycobacterium tuberculosis membrane vesicles inhibit T cell activation. J Immunol 2017;198:2028–2037.
60. Turner L, Bitto NJ, Steer DL, et al. Helicobacter pylori outer membrane vesicle size determines their mechanisms of host cell entry and protein content. Front Immunol 2018;9:1466.
61. Jiang Y, Kong Q, Roland KL, et al. Membrane vesicles of Clostridium perfringens type A strains induce innate and adaptive immunity. Int J Med Microbiol 2014; 304:431–443.
62. Mujahid S, Pechan T, Wang C. Improved solubilization of surface proteins from Listeria monocytogenes for 2-DE. Electrophoresis 2007;28:3998–4007.
63. Ho SS, Nahm MH. Lipoprotein lipase and hydrofluoric acid deactivate both bacterial lipoproteins and lipoteichoic acids, but platelet-activating factor-acetylhydrolase degrades only lipoteichoic acids. Clinical and Vaccine Immunology 2009;16:1187–1195.
64. Ho SS, Michalek SM, Nahm MH. Lipoteichoic acid is important in innate immune responses to gram-positive bacteria. Infect Immun 2008;76:206–213.
65. Uchida H, Machida M, Miura T, et al. A xenogeneic-free system generating functional human gut organoids from pluripotent stem cells. JCI Insight 2017;2: e86492.
66. Neufert C, Becker C, Neurath MF. An inducible mouse model of colon carcinogenesis for the analysis of sporadic and inflammation-driven tumor progression. Nat Protoc 2007;2:1998–2004.
67. Thaker AI, Shaker A, Suprada Rao M, et al. Modeling colitis-associated cancer with azoxymethane (AOM) and dextran sulfate sodium (DSS). Journal of Visualized Experiments 2012;67:4100.

68. Chen WW, Freinkman E, Wang T, et al. Absolute quantification of matrix metabolites reveals the dynamics of mitochondrial metabolism. Cell 2016; 166:1324–1337.e11.

Received June 15, 2023. Accepted January 16, 2024.

Correspondence
Address correspondence to: Motoyuki Otsuka, MD, Department of Gastroenterology, Graduate School of Medicine, The University of Tokyo, 7-3-1 Hongo, Bunkyo-ku, Tokyo 113-8655, Japan. e-mail: otsukamo-tky@umin.ac.jp; fax: +81-3-3814-0021.

CRediT Authorship Contributions
Yu Miyakawa, MD, PhD (Conceptualization: Equal; Data curation: Lead; Formal analysis: Equal; Writing – original draft: Lead)
Motoyuki Otsuka, MD, PhD (Conceptualization: Equal; Formal analysis: Equal; Writing – review & editing: Lead)
Chikako Shibata, MD, PhD (Data curation: Equal; Methodology: Equal)
Takahiro Seimiya, MD, PhD (Data curation: Equal; Formal analysis: Equal)
Keisuke Yamamoto (Resources: Supporting)
Rei Ishibashi, MD, PhD (Data curation: Supporting)
Takahiro Kishikawa, MD, PhD (Conceptualization: Equal; Data curation: Equal)
Eri Tanaka, MD, PhD (Data curation: Equal; Resources: Supporting)
Takayuki Isagawa, MD, PhD (Data curation: Supporting; Methodology: Supporting)
Norihiko Takeda, MD, PhD (Data curation: Supporting; Methodology: Supporting)
Noriaki Kamio, Dr (Resources: Equal)
Kenichi Imai, PhD (Resources: Supporting)
Mitsuhiro Fujishiro, MD, PhD (Writing – review & editing: Supporting)

Conflicts of interest
The authors disclose no conflicts.

Funding
Supported by Grants-in-Aid from the Ministry of Education, Culture, Sports, Science and Technology, Japan (#22H02828, #23KJ2162, #22K15958, #21K15916, and #21H02893) (to Motoyuki Otsuka, Chikako Shibata, Takahiro Seimiya, Rei Ishibashi, and Takahiro Kishikawa) and by the grant from Japan Agency for Medical Research and Development, AMED (JP23fk0310506 and 23fk0210092 to Motoyuki Otsuka) and from JST CREST (#JPMJCR19H5 to Motoyuki Otsuka).